A NEW APPROACH FOR SEISMIC INVERSION WITH GAN ALGORITHM

BEHNIA AZIZZADEH MEHMANDOST OLYA[1], REZA MOHEBIAN[*2], ALI MORADZADEH[3]

[1]School of Mining Engineering, College of Engineering, University of Tehran, Tehran, Iran
[2]Assistant Professor, School of Mining Engineering, College of Engineering, University of Tehran, Tehran, Iran, mohebian@ut.ac.ir, https://orcid.org/0000-0001-6516-7336
[3]Professor, School of Mining Engineering, College of Engineering, University of Tehran, Tehran, Iran,

(Received April 20, 2024; revised version accepted October 4, 2024)

ABSTRACT

Seismic surveying represents an efficient and pivotal tool in the exploration of hydrocarbon reserves, consistently drawing the focus of the upstream oil and gas industries. Seismic inversion, one of the most critical methods for delving into the characteristics of subsurface geological layers, poses a formidable challenge. In this study, we've departed from the conventional approach of merely enhancing or combining existing seismic inversion methods. Instead, we've employed a novel generative-adversarial network (GAN) algorithm, which is a deep learning algorithm, meticulously trained for the seismic inversion process. This innovative approach aims to omit several pressing challenges, including the computation of the inversion matrix, initialization of the wavelet, and navigating the constraints of the limited frequency band of seismic amplitudes in seismic inversion. This study has yielded remarkable results. Through the application of the generative-adversarial deep learning algorithm, we've not only conquered the aforementioned challenges but have also achieved exceptional quality and precision in our results. We conducted seismic inversion using real data from an oil field, achieving an impressive accuracy rate of 97.5%. This accuracy percentage is validated based on both the validation data and the mean squared error (MSE), reinforcing the robustness of the proposed approach. Furthermore, the acoustic impedance of the five test wells consistently measured below 0.125 units, highlighting the excellence of our outcomes. The correlation coefficient among these test wells ranged from a minimum of 96% to a maximum of 99%. In contrast, the acoustic impedances obtained through the band-limited method and the model base method displayed correlation coefficients of 71% and 83%, respectively. The utilization of the generative-adversarial algorithm in the inversion process underscores its contemporary efficiency. It holds the potential to entirely modernize and refine the conventional seismic inversion process, ushering in a new era of seismic exploration and inversion.

KEY WORDS: Seismic Inversion, generative-adversarial network (GAN) algorithm, Deep Learning, Seismic Exploration, Seismic Reservoir characterization

0963-0651/23/$5.00

INTRODUCTION

The exploration for hydrocarbon reserves has been a driving force behind the evolution of geophysical techniques, particularly seismic methods (Russell, 1988; Chopra & Marfurt, 2005). Accurately imaging and characterizing subsurface structures is pivotal in locating and assessing hydrocarbon reservoirs (King, 1992; Mallick, 1995). The foundation of seismic exploration was laid by seminal work in theoretical seismology. Researchers like Ludger Mintrop and Eckhardt conducted experiments involving artificial seismic sources, providing valuable insights into subsurface structures using explosives to generate seismic waves in 1949 (Mintrop, 1949; Sheriff & Gedart, 1995). The widespread adoption of reflection seismology gained impetus during the mid-20th century due to significant advancements in digital recording equipment and the concurrent realization of its profound potential in facilitating the detailed imaging of subsurface geological structures, Notably, the seismic inversion process is inherently intricate and time-consuming, owing to the substantial volume of data required for its computations. Consequently, numerous challenges inevitably arise throughout the course of seismic inversion (Russell, 1988; Yilmaz, 2001). Simultaneously, seismic inversion techniques began to emerge in response to the demand for quantitative subsurface information. Early inversion efforts, such as the limited band inversion method, sought to derive simple attributes like acoustic impedance from seismic data (Ferguson & Margrave;1996; Helgesen, et al., 2000; Maurya & Singh, 2017). As the journey of extensive research on seismic inversion persisted, it unveiled a series of novel methods, each distinguished by its unique attributes. The base and sparse spike model, which aimed to represent subsurface properties as a series of spikes in depth, marked a significant departure from linearized approximations (Ji, Yuan, & Wang, 2019;Kushwaha,et al., 2020). This method laid the foundation for modern seismic inversion approaches, incorporating the full wave equation and utilizing optimization techniques. The late 20th century and early 21st century saw a convergence of advanced computing power, sophisticated algorithms, and high-quality data acquisition systems. This synergy led to the development of 3D and 4D seismic surveys, allowing for the imaging of subsurface structures with unprecedented detail. Seismic inversion evolved alongside these advances, with techniques such as full-waveform inversion (FWI) gaining prominence (Virieux & Operto, 2009; Xu, etal., 2012 ; Lin, et al., 2023;Azizzadeh Mehmandost Olya, et al.,2024a).

As previously mentioned, multiple algorithms have been devised to delegate this task to computers. The critical consideration lies in the fact that these algorithms lack the capacity to learn or exhibit intelligent behavior. Consequently, their parameters necessitate manual adjustment for each instance by an operator. Additionally, when faced with challenges during the inversion process, these algorithms lack the ability to automatically resolve issues. Furthermore, it is important to note that certain conventional seismic inversion algorithms are susceptible to noise, which leads to the propagation

of errors throughout the inversion process (Gogoi & Chatterjee, 2019; Zhang, et al,. 2023; Lin et al., 2023). Owing to their remarkable capabilities, deep learning algorithms present a highly promising avenue for the implementation of intelligent techniques in seismic inversion. These sophisticated algorithms hold the potential to revolutionize the entire seismic inversion process. Deep learning has garnered increasing popularity in recent years for its remarkable capabilities when applied to the exploration of hydrocarbon reserves (Bagheri, et al; 2024;Moradi Chaleshtori,et al.,2024 ;Bahramali Asadi Kelishami & Mohebian, 2021;Mohebian, et al.,2021). This cutting-edge technology is revolutionizing the way we approach the task of identifying and assessing these valuable natural resources. Its rising prominence can be attributed to several key factors (Zhu, et al., 2022).

Firstly, deep learning algorithms excel at processing vast and complex datasets, a critical requirement in the subject of hydrocarbon exploration. With the ability to analyze seismic data, geological formations, and subsurface conditions with unprecedented accuracy, deep learning enhances our capacity to pinpoint potential reserves and predict their viability (Azizzadeh Mehmandost Olya,et al., 2024b ; Rajabi, et al., 2019). Secondly, the adaptability of deep learning models makes them invaluable in tackling the inherent challenges of hydrocarbon exploration. These algorithms can continuously evolve and improve their predictive capabilities as they learn from new data, making them highly efficient in adapting to evolving geological conditions and exploration techniques (Geng & Wang, 2020; Habibullah, et al., 2020). Within the realm of hydrocarbon reserve exploration (Azizzadeh Mehmandost Olya & Mohebian, 2023a) and the intricate analysis of seismic recordings, deep learning algorithms have garnered extensive utilization, underscoring the distinctive prominence of this algorithmic category (Azizzadeh Mehmandost Olya & Mohebian, 2023b).

In this paper, we employed the Cyclic generative adversarial network (GAN) deep learning algorithm. This algorithm represents a cutting-edge approach, distinguished by its unique capabilities. Its inception dates back to 2014, credited to Ian Goodfellow (Goodfellow, et al., 2014). Presently, the algorithm boasts several distinct architectures, signifying its ongoing developmental trajectory. The primary impetus behind the creation of this algorithm has been the generation of lifelike images. Remarkably, this algorithm has the capacity to fashion images previously nonexistent, subsequent to undergoing multiple rounds of training and exposure to diverse visual stimuli (Frank, et al., 2020). As this algorithm matured, Xu and his colleagues successfully adapted it to tabular data in 2019, thereby underscoring its versatility beyond image data (Xu, et al., 2019). Subsequently, in 2020, Liu and his research team achieved a remarkable feat by employing the GAN algorithm to construct a model for weather estimation and forecasting. This accomplishment underscores the algorithm’s extraordinary computational prowess (Liu & Lee, 2020). Within this article, we harnessed the GAN algorithm to produce sonic and density logs,

facilitating seismic inversion through a novel approach. Notably, this approach not only circumvents the typical challenges posed by conventional methods but also enhances accuracy and expedites the process significantly.

METHODOLOGY

The GAN is a sophisticated deep-learning algorithm that offers various variants tailored for specific purposes. In this article, we employ the cyclic variant and will proceed to elucidate its architecture (Creswell, et al., 2018; Aggarwal, et al., 2021).

Algorithm Architecture

The GAN algorithm essentially comprises two distinct sub-networks that operate concurrently. This interplay between the two sub-networks facilitates a more precise training of the desired models and commands (Gui et al., 2021). A fitting analogy to elucidate this algorithm is that of a counterfeiter and a detective. In a hypothetical mental realm, the counterfeiter strives to craft the most convincing counterfeit money, while the detective endeavors to discern counterfeit money from genuine currency. Through a communication channel, the detective informs the counterfeiter whether the counterfeit money has been identified. If the counterfeit money is detected, it indicates that the counterfeiter requires further refinement in their craft, and the detective is effectively performing their role. Conversely, if the detective fails to accurately distinguish the counterfeit money, it implies a need for more training on their part. Ultimately, the optimal state is achieved when the counterfeiter cannot enhance the similarity of their counterfeit money to real money any further, and the detective cannot differentiate the counterfeit money from genuine currency due to their closely matched characteristics. The example presented essentially illustrates two core sub-networks: the generative and the adversarial. The generative network enhances the accuracy of its outcomes by creating requested samples and forwarding them to the adversarial network, which in turn endeavors to identify errors within the transmitted samples. Furthermore, within the framework of this generative network algorithm, the network strives to learn the underlying concepts of the specified subject. This dynamic signifies that the network possesses the capability to generate authentic data that previously had no existence (Karras, et al., 2020). In figure 1, we have depicted a simplified flowchart of the GAN algorithm. This flowchart illustrates what we mentioned earlier, specifically the relationship between the generative subnet and the adversarial subnet. In this figure, we can observe that when the data generated by the generating sub-network conflicts with reality, the adversarial network prompts for the regeneration of the data.

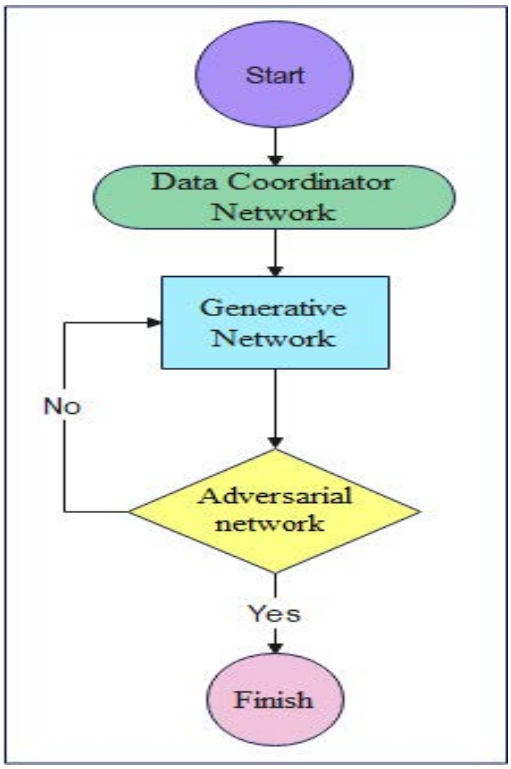

Figure 1—Simplified flowchart of GAN algorithm

Sub-Networks

The diversity of algorithms in GAN sub-networks depends on their goals, and the choice of algorithms is crucial for effective learning. In this article, we used fully connected neural networks for both the generative and adversarial sub-networks. The generator network utilized the Rectified Linear Unit (ReLU) activation function to emphasize nonlinear relationships.

This variety of algorithms in GAN sub-networks allows for a tailored approach, enabling customization for specific tasks. Our use of fully connected neural networks in both sub-networks supports comprehensive information exchange within the model's architecture. Integrating the ReLU activation function into the generator network enhances the model's ability to capture complex data patterns.

The careful selection of algorithms reflects the meticulous design in GANs, where the synergy between components significantly influences the system's performance. Before discussing the loss functions governing these sub-networks, it's essential to understand the concept of Nash equilibrium, a crucial foundation for comprehending convergence in responses.

Nash Equilibrium

Nash Equilibrium, a foundational concept in game theory, is a state in which

each participant's strategy is optimal, given the strategies chosen by all other participants. Mathematically, in a strategic interaction involving multiple players, let's denote the strategy of player (i) as S_i, and the set of strategies of all players except (i) as S_{-i} The payoff to player (i) for playing strategy S_i while others play strategies from S_{-i} is denoted as U_i (S_i, S_{-i}). A Nash Equilibrium is reached when no player has an incentive to unilaterally change their strategy, i.e., for all players (i) the following condition holds:

$$U_i\,(S_i, S_{-i}) > U_i\,(S'_i, S_{-i}) \quad (1)$$

for all possible alternative strategies $S'_i$of player (i) and all combinations of strategies S'_i of other players. In simple terms, each player's strategy is the best response to the strategies of others.

In the context of Generative Adversarial Networks (GANs), the concept of Nash Equilibrium manifests intriguingly. GANs consist of two primary sub-networks: the generator and the discriminator. The generator creates data instances, while the discriminator (Adversarial) evaluates whether a given instance is real (from the actual data distribution) or fake (generated by the generator). This interaction resembles a game between the generator and discriminator. The generator seeks to generate data that the discriminator cannot easily differentiate from real data, while the discriminator aims to accurately classify real from fake data.

Mathematically, the discriminator's strategy involves producing an optimal decision boundary, and the generator's strategy entails creating data that can effectively deceive the discriminator. The equilibrium in this context is the state in which the generator produces data that is so realistic that the discriminator can't distinguish it from real data, while the discriminator's classification accuracy remains around 50%, as it cannot confidently discern between the two.

Achieving Nash Equilibrium in GANs is a non-trivial task. If the generator becomes too adept, the discriminator might falter in improving its own accuracy, and vice versa. This tug-of-war often leads to oscillations in training and convergence challenges. Researchers have developed various strategies to stabilize training, like introducing mini-max game formulations and adjusting learning rates.

Loss function

The core of GANs lies in the intricate interplay between two neural networks: the generator and the discriminator. This interaction is orchestrated by meticulously designed loss functions that drive the training process, leading to the convergence of these networks.

- Generator Loss: The generator's primary objective is to create data

samples that are indistinguishable from real data. To achieve this, the generator loss function encourages the generator to produce data that the discriminator misclassifies as real. Mathematically, the generator loss (L_G) is given by the negative logarithm of the discriminator's probability of correctly identifying generated data as fake ($L_G = -\log\big(D(G(z))\big)$), where $G(z)$ represents the generator's output given noise input z.

- Discriminator Loss: The discriminator aims to accurately differentiate between real and generated data. Its loss function (L_D) is devised to maximize its ability to discriminate. It consists of two components: the negative logarithm of the discriminator's probability of correctly classifying real data as real ($-\log(D(x))$) and the negative logarithm of the discriminator's probability of incorrectly classifying generated data as real ($-\log\big(1 - D(G(z))\big)$).

- Adversarial Minimax Game: GAN training can be viewed as a two-player minimax game, where the generator and discriminator are adversaries. The generator's goal is to minimize its loss while the discriminator aims to maximize its loss. This adversarial objective is mathematically expressed as $\min(G)\max(D[L_D + L_G])$.

- Equilibrium and Nash Equilibrium: The equilibrium of this adversarial game occurs when both the generator and discriminator reach a point where neither can improve by unilaterally changing its strategy. This equilibrium is akin to a Nash equilibrium in game theory, where the generator produces data that is realistically mistaken for real by the discriminator.

Seismic inversion process with GAN algorithm

Seismic inversion stands as one of the paramount methodologies for exploring hydrocarbon reserves and subterranean water sources. Nonetheless, conventional techniques like the limited band and the model-based methods confront an array of fundamental challenges. These challenges encompass wavelet extraction, constraints on data bandwidth, intricate matrix calculations (ill-condition matrix), and the omnipresent issue of data noise.

In this paper, we introduce a novel approach to seismic inversion aimed at circumventing these obstacles. Our chosen approach employs the GAN algorithm. In stark contrast to prior methods that sought to extract acoustic impedance from seismic traces, our approach involves the creation of acoustic impedance directly from these traces. In essence, at each location where a seismic trace is present, we obtain two logs which are a density log and a sonic log. This innovative technique eliminates the need for wavelet generation via diverse statistical methods. Moreover, it obviates the reliance on matrix inversion for seismic inversion, thereby sidestepping the associated matrix inversion issues.

Furthermore, the unique capabilities of the GAN algorithm afford us the added advantage of mitigating noise effects during the inversion process.

Consequently, this approach represents a promising breakthrough in the field of seismic inversion, addressing key challenges and enhancing the precision of hydrocarbon reserve and underground water source exploration.

In Figure 2, a meticulously detailed flowchart unfolds, a visual representation of the primary methodologies and key processes that underpin this article's pursuit of seismic inversion has been provided. The integration of the GAN algorithm into the seismic inversion framework is made explicit through this visual exposition, offering readers a deeper understanding of the intricate steps involved in this innovative approach. In the upcoming section, our objective is to provide a comprehensive elucidation of the distinct elements comprising this intricate flowchart. Through a detailed breakdown of each component, we aim to offer a clear and thorough understanding of the visual representation presented herein.

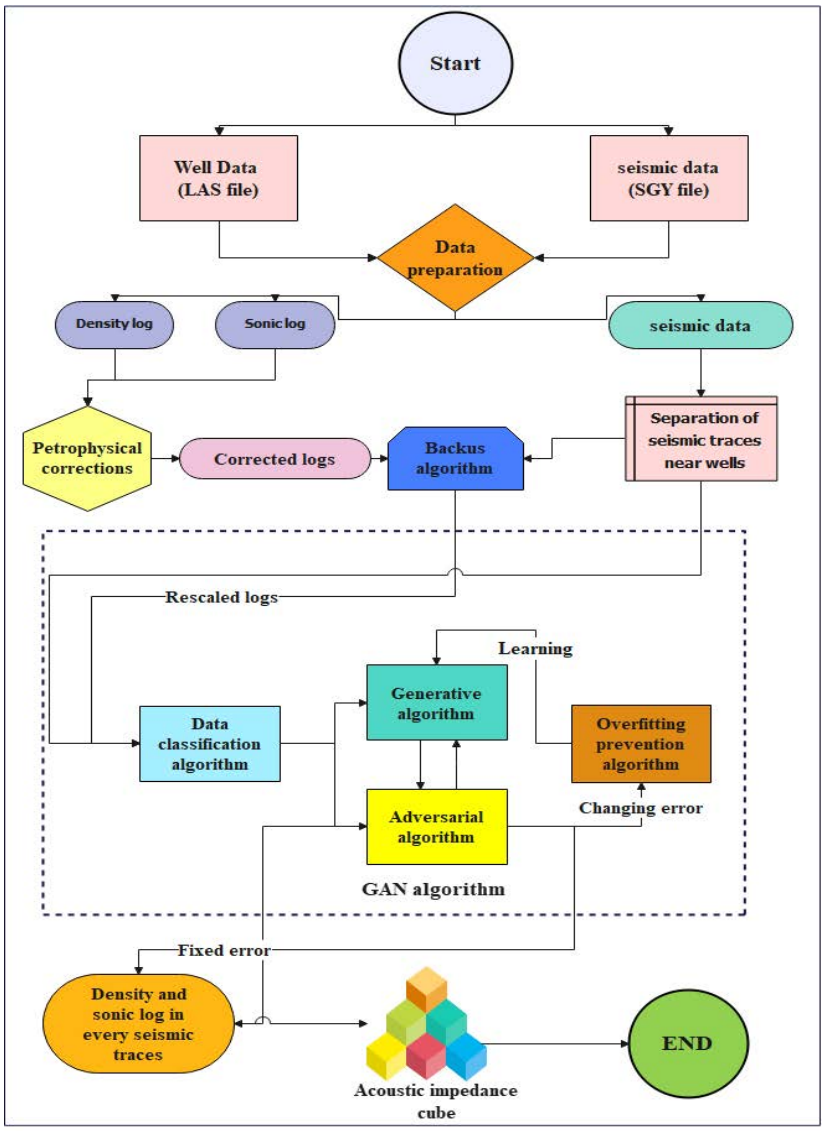

Figure 2—Flowchart of seismic inversion by GAN algorithm

Data preparation

We use two primary data categories in this approach: seismic data and well log data. Python is our chosen programming language due to its open-source nature and its capability to handle complex deep-learning algorithms.

During the initial stages of this article, retrieving seismic and well data is crucial. Given the significant volume of seismic data, we implement a data batching technique. This technique serves a dual purpose: it reduces the number of data packets sent to the graphics processing unit and the primary code kernel, thereby preventing potential memory overflow in the computer. This process is part of the "Data preparation" section. Table 1 presents a pseudocode that thoroughly explains the data batching process, providing insights into the systematic steps for efficient organization and processing of data in discrete segments.

Table 1—Batching pseudocode

```
function batch_large_file(input_file_path, output_directory, chunk_size)
    if not exists(output_directory)
        create_directory(output_directory)

    input_file = open (input_file_path, 'read_binary')
    chunk_number = 1

    while True
        chunk_data = read_chunk(input_file, chunk_size)
        if chunk_data is empty
            break

        output_file_path = create_output_file_path(output_directory, chunk_number)
        output_file = open (output_file_path, 'write_binary')
        write_chunk(output_file, chunk_data)
        close(output_file)

        increment(chunk_number)

    close(input_file)

if __name__ == "__main__"
    input_file_path = "path/to/your/large/file.dat"
    output_directory = "path/to/output/directory"
    batch_large_file(input_file_path, output_directory)
```

Another crucial consideration is the unique formatting of seismic data files (SGY format) and well-log data files (LAS format). These files undergo a sophisticated encryption process that significantly reduces the storage requirements for seismic and well-log data. As a result, conventional methods

for accessing these files are ineffective. To overcome this encryption challenge and access the valuable seismic and well-logging datasets, we developed a specialized pseudocode tailored to the distinct encryption methods and characteristics of SGY and LAS files. Table 2 provides this pseudocode, serving as a vital link between the intricate data encryption and our analytical processes.

Table 2—opening file algorithm

```
Procedure: Open SGY Seismic Data and LAS Well Logging Files

Input:
  - sgy_file_path: The path to the SGY seismic data file
  - las_file_path: The path to the LAS well logging file

Output:
  - seismic_data: The seismic data loaded from the SGY file
  - well_log_data: The well logging data loaded from the LAS file

1. Specify the path to the SGY seismic data file as sgy_file_path.
   Specify the path to the LAS well logging file as las_file_path.

2. Load the SGY file using the sgysak package:
   - Initialize seismic_data as an empty variable.
   - Use the sgysak package to read the SGY file located at sgy_file_path and store the data
in seismic_data.

3. Access header information and seismic trace data if needed:
   - Extract header information from seismic_data.header.
   - Extract seismic trace data from seismic_data.traces.

4. Load the LAS file using the lasio package:
   - Initialize well_log_data as an empty variable.
   - Use the lasio package to read the LAS file located at las_file_path and store the data in
well_log_data.

5. Access header information and well log data if needed:
   - Extract header information from well_log_data.header.
   - Extract well log data (curves) from well_log_data.data.

6. End the procedure.
```

Petrophysical corrections

Upon gaining access to the dataset, a critical task emerges: the isolation of seismic trace data closely associated with the existing wells. To execute this task with precision, we initiated the process by acquiring accurate geographical coordinates for each wells. Using this geographical data, we then meticulously delineated and separated the seismic traces that corresponded to the wells

in closest proximity within the expansive seismic dataset. This meticulous approach ensures that our subsequent analyses and computations are grounded in the most relevant and contextually significant data points.

Following the extraction of seismic trace data closest to point of interest, our focus shifts towards the crucial task of refining the well log data from a petrophysical perspective. In this study, we have exclusively harnessed sonic and density logs as our primary sources, opting not to directly incorporate other logs types into our analysis. We recognize that the post-drilling conditions within wells are subject to variability and instability. Factors such as localized wall collapses or the potential intrusion of drilling mud can introduce significant irregularities into the well's internal structure. Consequently, during the deployment of well logging tools, we often contend with the complexity of a non-uniform well wall.

Moreover, each well logging tool necessitates specific adjustments. For example, when dealing with the sonic log, a critical petrophysical correction known as the "double circulation correction of sound waves," or simply "d-spike," takes center stage. This correction serves to eliminate aberrations associated with acoustic double circulation, effectively smoothing out the recorded log data and rendering it more coherent and scientifically sound.

As mentioned earlier, the propensity for well wall collapses is a genuine concern. In instances where such incidents occur, the well log data obtained in proximity to the compromised well wall loses its validity. To tackle this issue head-on, we have meticulously purged the dataset of values originating from regions adjacent to the affected well wall. To bridge the ensuing data gaps, we've employed a rigorous averaging technique, thus ensuring the continuity and integrity of the dataset.

Yet another formidable challenge revolves around the disparity in depth alignment across various well logging datasets. This means that values corresponding to a specific geological layer may exhibit variations in depth measurements. To mitigate this misalignment, we've adopted the gamma ray log as a reference point. This reference serves as the essential for our efforts to harmonize the depth measurements across all logs, effectively resolving the issue of depth mismatch and enhancing data consistency for our comprehensive analysis.

Backus algorithm for upscaling

After the meticulous correction of petrophysics log data and the meticulous separation from the closest trace to the well data, we confront one of the most pivotal challenges in our quest for data alignment and synergy. It's essential to recognize that well logging devices diligently record data points at an interval of 0.1524 meters, whereas seismic sampling captures data at substantially

wider intervals. Consequently, connecting these two disparate data streams necessitates a concerted effort. Before we embark on this endeavor, it becomes imperative to address the fundamental issue of scale discrepancy between well logging and seismic data. The wellbore data is inherently expressed in meters, whereas seismic data is inherently associated with milliseconds. To tie this divide and establish a common scale, we rely on the invaluable resource of check shot data. Check shot data serves as the linchpin in harmonizing these distinct scales, allowing for seamless conversion between the meter and millisecond domains with precision. Our overarching objective, which is to perform a seismic data inversion, hinges on the seamless alignment achieved through this process. To obtain well data that aligns with the seismic scale, we employ a carefully crafted formula, meticulously derived from curve fitting to the check shot data (as depicted in Figure 3). This formula serves as a bridge that ensures our seismic data inversion efforts are underpinned by accurate and synchronized borehole data.

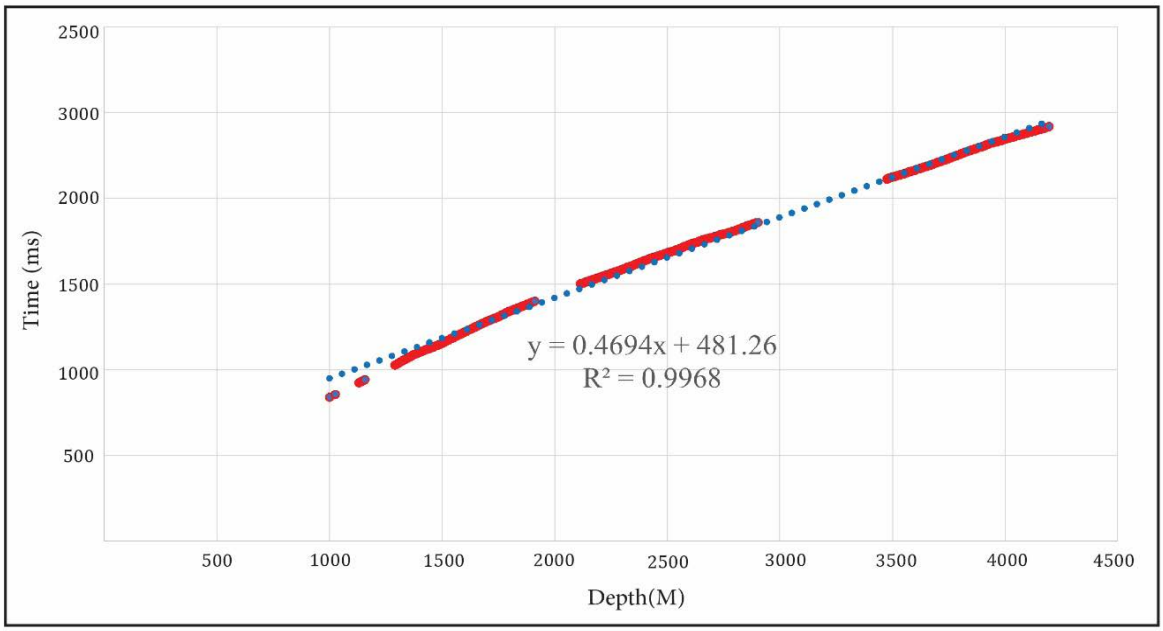

Figure 3—Curve fitting on check shot data

Following the successful utilization of check shot data to effectuate the conversion of borehole data from “meters” to “milliseconds,” our next imperative lies in establishing a seamless connection between this transformed borehole data and the seismic dataset. To achieve this, we turn to an ingenious method introduced by George Backus back in 1962, known as the Backus mean (Backus, 1962).

The Backus mean method provides us with a powerful framework for establishing the crucial link between well log data and seismic data. It offers a systematic approach through which these two disparate datasets can be meaningfully related and analyzed. This method serves as a vital bridge that facilitates the fusion of well log data and seismic data, ultimately enhancing our ability to interpret and inversion seismic data (Figure 4).

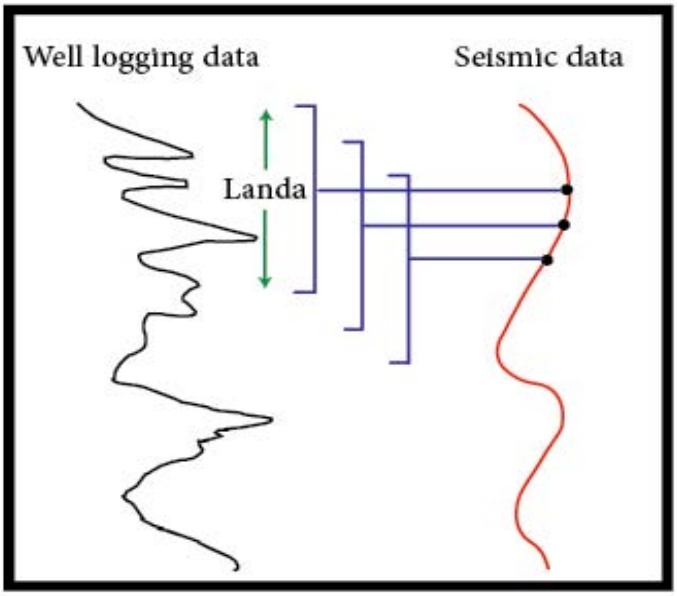

Figure 4—Backus mean

Within the framework of the Backus algorithm, a crucial parameter known as the Landa value defines the temporal extent of the window within which well data becomes intimately integrated and correlated with seismic data. This window's length is intrinsically tied to the temporal characteristics of the recorded seismic data. To illustrate, if there is a 2.5-millisecond gap between each recorded seismic domain, the corresponding window length will precisely mirror this 2.5-millisecond interval.

This meticulous synchronization between the seismic data's recording time intervals and the Landa value underpins the algorithm's effectiveness. Moreover, the conversion of well-logging data into the "milliseconds" scale facilitates a harmonious fit within this window. This harmonization ensures that the window operates seamlessly, enabling the precise alignment and association of well data with its seismic counterpart.

Calibrating the scale of seismic and well data

In the previous section, we discussed the working method of Backus averaging. It's important to note that one of the challenges associated with this averaging technique is the lack of accurate matching between the time domains of well data and seismic data. This discrepancy can be observed in Table 3.

Table 3—The Non-Uniformity of Time Domains of Well and Seismic Data

Well Time Domain (milliseconds)	Seismic Data Time Domain (milliseconds)
102.262	100.508
102.473	104.221
102.658	107.207

As seen, there is an incomplete match between the seismic amplitudes and the well data due to various factors, including environmental conditions and device accuracy. To address this challenge, we implemented a calibration process that aligns the well's time domain with the seismic data. Here's a step-by-step description of the process:

1. Initially, we select the closest seismic trace to the well being investigated as the reference data.

2. Next, we calculate the difference between all seismic trace time domains and the well data time domains.

3. The data pair with the smallest difference is chosen as the reference time point.

4. We adjust the time domain within the well logging data based on the difference between the well and seismic time domains.

5. We recalculate the time difference between the seismic trace and the updated well logging time domain. Notably, the previously calculated and adjusted data pairs remain fixed, while only the well's time domain is updated. This ensures accurate recording of seismic amplitudes at layer boundaries during processes such as "Z crossing" or "S crossing."

6. In this step, we add or subtract a quarter of the calculated difference to the well logging time domain. This approach prevents unrealistic adjustments that could occur if the entire difference were applied across the entire range of well logging data simultaneously.

7. We repeat this process until no pair of time-domain seismic and well log data can be further optimized.

Through this iterative process, the difference between the well data's time domain and the seismic acquisition time domain is minimized, leading to more accurate results after Backus averaging

Data classification algorithm

Within the scope of this research endeavor, our data set comprises a total of 15 wells and a singular seismic cube. For our analysis and evaluation, we segregated 5 wells from the dataset, selected based on their distinct dispersion characteristics, earmarking them for use in our testing phase. The remaining 10 wells were designated as training data.

Crucially, the effective training of algorithm necessitates the meticulous classification and arrangement of these data points in conjunction with the data from the closest seismic trace. This approach ensures that, during the algorithm's training phase, each data point is thoughtfully aligned with similar data, enhancing the learning process.

To achieve this goal, we employed a well data sorting algorithm in tandem with the closest seismic trace information. This meticulous sorting process serves as the foundation for constructing a training feed for both the generator sub-networks and the adversarial sub-network. By organizing the data in this manner, we optimize the algorithm's capacity to recognize patterns, relationships, and nuances, ultimately leading to more robust and accurate results in our exploration and analysis.

GAN algorithm for seismic inversion

In contrast to traditional seismic inversion methods, this research takes a unique approach by directly performing inversion operations on seismic traces without the need to extract wavelet or intermediate operator information beforehand. We've already detailed the meticulous data preparation steps for this study. Now, let's delve into the subsequent phase, where we send this carefully prepared data into two essential sub-networks: the generator sub-network and the adversarial sub-network. The generator sub-network has the challenging task of learning and deciphering the intricate relationship between well data and their nearest seismic trace counterparts. It serves as the creative force behind generating synthetic models. On the other hand, the adversarial sub-network acts as the discerning critic, tasked with distinguishing between these synthetic models and the authentic ones derived from real data. Essentially, the adversarial sub-network works to refine and enhance the generative algorithm by progressively recognizing the subtle discrepancies and shortcomings inherent in the synthetic models produced by the generative sub-network. This iterative process continues until the adversarial algorithm achieves the remarkable ability to discern synthetic models from genuine ones, driving the generative algorithm to produce increasingly accurate and realistic models.

This dynamic interplay between the generative and adversarial sub-networks forms the core of our innovative approach to seismic inversion, promising to advance the boundaries of accuracy and realism in model generation and data interpretation. Now, let's discuss the loss function for the GAN, which comprises two components ;the generator loss and the discriminator loss. GANs are employed in semi-supervised deep learning to train a generator network (G) and a discriminator network (D) simultaneously. The primary objective is for the generator to produce data that is indistinguishable from real data, while the discriminator aims to differentiate between real and generated data. Here's the mathematical representation of the GAN loss function:

1. Discriminator Loss (D_{loss}):

The discriminator's loss measures its ability to distinguish between real and generated data.

$$D_{loss} = -\left[log(D_{real\ data}) + log(1 - D_{generated\ data})\right] \quad (2)$$

Where $D_{real\ data}$represents the probability assigned by the discriminator to real data being real. $D_{generated\ data}$ signifies the probability assigned by the discriminator to generated data being real.

The discriminator's goal is to maximize D_{loss}, meaning it aims to correctly classify real data as real ($D_{real\ data}$close to 1) and generate data as fake ($D_{generated\ data}$ close to 0).

2. Generator Loss (G_{loss}):

The generator's loss measures how effectively it can deceive the discriminator.

$$G_{loss} = -\log(D_{\ generated\ data}) \quad (3)$$

The generator's objective is to minimize G_{loss}, implying that it strives to generate data so convincing that the discriminator assigns a high probability to it being real ($D_{generated\ data}$ close to 1).

In practice, GAN training involves alternating between optimizing the discriminator and the generator by minimizing their respective loss functions. The generator seeks to enhance its ability to generate realistic data, while the discriminator aims to improve its ability to distinguish between real and generated data. The overall GAN loss is typically represented as the sum of the discriminator loss and the generator loss:

$$Loss_{totall} = D_{loss} + G_{loss} \quad (4)$$

The GAN training process aims to achieve a Nash equilibrium between the generator and the discriminator, where the generator produces realistic data, and the discriminator cannot reliably distinguish between real and generated data. This equilibrium is reached through iterative training, with both networks continuously improving their performance. Within the realm of GANs, a crucial component is the data classifier algorithm. Its primary role is to ensure the precise alignment of well data and seismic traces, forming the foundation for the GAN process.

Once alignment is established, the data classifier algorithm acts as a conduit, providing both well log and seismic trace data to the generative algorithm for training. Simultaneously, it supplies the same dataset to the adversarial algorithm, setting the stage for a dynamic "minmax game." In this intricate interplay, the generator algorithm generates genuine data, while the adversary algorithm scrutinizes its authenticity. To address the risk of overfitting, a proactive approach is employed. An algorithm is meticulously designed to prevent overfitting by controlling the neural elements of the generating network, ensuring that all neurons do not converge towards optimization within

a single epoch. This measure enhances the algorithm's robustness. The training process continues until the error metrics between the adversarial and generative algorithms stabilize, making neither algorithm the clear victor. Subsequently, armed with detailed information about each seismic trace, the generator algorithm generates density, and sonic logs. This results in a comprehensive dataset encompassing sonic logs and acoustic impedance profiles at the precise geographic coordinates of each seismic trace.

This marks the culmination of the inversion process, a complex endeavor that underpins seismic data interpretation and modeling. The GAN algorithm's capability to not only generate data but also modify existing data sets it apart from other deep learning methods. The GAN framework, with its interplay of algorithms, represents a sophisticated and innovative approach that advances the boundaries of data generation, interpretation, and modeling within the realm of seismic analysis and beyond.

The GAN algorithm developed for seismic inversion is a sophisticated approach employing a fully connected neural network. Within the generative subnet, there are three layers, each with 1500 neurons. This specific configuration was carefully chosen to handle the inherent complexity of seismic data, and it went through extensive trial and error to capture the intricate patterns and nuances present in the data effectively.

In the context of this research, the choice of the Rectified Linear Unit (ReLU) activation function for the generative algorithm is particularly noteworthy. This decision was motivated by its demonstrated ability to seamlessly align with seismic data characteristics, as evidenced by findings from Wang et al. (Wang, et al , 2022) This activation function plays a pivotal role in shaping the network's ability to extract meaningful features from the data, thereby enhancing the quality and accuracy of the generated results.

To understand the GAN algorithm's inner workings, we'll outline its key stages. The algorithm begins with "Input Gathering," where it collects necessary input parameters and data. This stage sets the groundwork. Next is "Generator Model Creation," where the algorithm constructs the generative model, taking into account the gathered input. This shapes the algorithm's capabilities. Following this, the algorithm moves to "Layer Specification," where it defines the network's architecture by specifying layer shapes and dimensions. These specifications are crucial for the model's effective functioning. After this, we have "Layer Creation," where the individual layers within the network are brought to life, aligning with the intended design. Moving forward, the algorithm focuses on "Input Integration," harmoniously merging inputs from various layers to facilitate data flow. It then "Adds Connected Layers," fostering synergy between layers for collective processing of input data. The chosen activation function, ReLU, introduces non-linearity, enhancing the network's ability to capture complex patterns in the data.

The number of layers doesn't follow a fixed pattern; it's "Iterative Layer Addition," ensuring adaptability to data intricacies. The algorithm reaches "Output Layer Definition" to specify the output layer, aligned with research objectives. Incorporating this layer finalizes the network's architecture, ensuring the model's output aligns with the research goals.

The result of these steps is the "Final Generative Model," encompassing both input and output layers. The process concludes with "Returning the Generator Model," delivering a fully equipped generative model, ready to generate valuable seismic inversion results.

The ReLU activation function, known for its simplicity and effectiveness, introduces non-linearity into neural networks. It efficiently models complex data relationships, making it suitable for applications like seismic inversion, where it excels in capturing intricate data patterns. ReLU is a non-linear activation function that introduces non-linearity into the neural network. Unlike some other activation functions like the sigmoid or hyperbolic tangent (tanh), ReLU has a simple mathematical formulation: it outputs the input value if it's positive and outputs zero if it's negative (Figure 5).

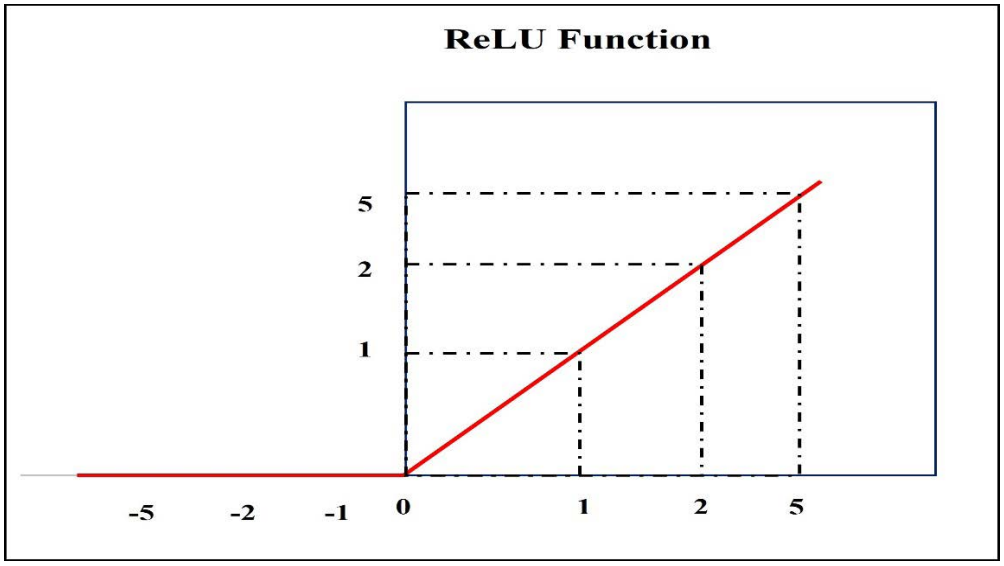

Figure 5—ReLU activation function

In this research, the adversarial algorithm has been designed with the specific goal of estimating data from sonic and density logs. Within this algorithm, we employed a neural network architecture comprising three fully connected layers. The first layer consists of 512 neurons, the second layer is equipped with 256 neurons, and the final layer is a single neuron.

This approach was chosen to train the Adversarial algorithm effectively, aligning it with the precise requirements of estimating data from acoustic and density borehole logs. The neural network's architecture, with its layered structure and varying neuron counts, is meticulously crafted to capture and interpret the intricate patterns and relationships present in the data. This

design allows the algorithm to distill meaningful insights and deliver accurate estimates, ultimately enhancing the quality of results in the context of well log analysis.

In the preceding sections, we provided a comprehensive overview of the objective functions employed in the generative-adversarial algorithm. In this section, our focus shifts to the examination of the objective function tailored specifically for seismic inversion. Broadly, the proposed approach encompasses two distinct objective functions: one dedicated to the generative algorithm and another associated with the inversion algorithm.

Within the framework of the generative algorithm, we encounter a nuanced process designed to mitigate errors and streamline computational efficiency. This process aims to prevent the simultaneous, unsupervised input of both acoustic and density images into the adversarial network, thereby managing the computational load and minimizing processing time. Initially, this involves error computation through the generation of a profile, achieved by leveraging the closest seismic data points to the well, along with sonic and density well log data. The following equation exemplifies the initial step, where the first sonic and density logs (acoustic impedance) are derived from the profiles of the corresponding well and the nearest seismic trace to the well.

$$L_{G1}(W_{b1}, W_F) = \left|\left|T^* - \left(P_{W_F}(T^*) + f_L\right) - (PW_F(T) + f_L)\right|\right| \tag{5}$$

Upon the successful completion of the initial cycle for generating well data, the second objective function comes into play. This objective function is dedicated to the task of reconstructing well data utilizing seismic data. In essence, it initiates a local inversion process, and the subsequent equation illustrates this particular cycle.

$$L_{G2}(W_{b2}, W_F) = \left|f_H - P_{W_b}\left(f_{W_F}(f_H + f_L)\right)\right| \tag{6}$$

In the equations presented above, two critical weight functions are denoted: W_b,representing the local inverse model, and W_F, symbolizing the forward modeling process. The variable (T) stands as the seismic data, signifying the data originating from the seismic range nearest to the well. Within the equation framework, the symbol (P) denotes a function, with its index representing either the weight function of the local inverse model or the forward modeling process. It is essential to note that f_H and f_L correspond to high-frequency and low-frequency acoustic impedance data, respectively. These acoustic impedance values result from the analysis of sonic and density logs, where Fourier series is instrumental in their separation.

The rationale behind segregating these two datasets, rather than combining them, and presenting them individually to the algorithm lies in the pursuit of heightened accuracy and spatial resolution. We amalgamated the datasets, and the inherently diverse nature of high-frequency data in the density

and sonic log would have significantly marginalized the contribution of low-frequency data in computational calculations.

The loss function within the adversarial algorithm is:

$$L_D = log(T) + log(T^*) + log\left(1 - P_{W_D}\left(P_{W_F}(f_H + f_L)\right)\right) \quad (7)$$

In all of the relationships mentioned above, the variable (T) signifies seismic data from locations other than those in close proximity to the well. Conversely, T^* is used to denote seismic data collected near the well. It's worth noting that W_D pertains to the weight functions employed within the cleaning algorithm. This clarification distinguishes between the two datasets represented by T and $T^*$and highlights the significance of the weight functions encapsulated within the cleaning algorithm.

RESULTS AND DISCUSSION

We had a total of 15 wells at our disposal, out of which 10 were dedicated to the training of GAN algorithm. The remaining quintet served as test data repositories, essential for gauging the algorithm's performance. It's imperative to underscore that each training well, along with its closest seismic trace, contributed 80% of its data to the training process, while the remaining 20% played a pivotal role in the validation phase. This validation procedure was seamlessly integrated into the algorithm's ongoing training regimen.

The convergence validation values generated by the algorithm provide a clear and quantitative reflection of its accuracy. These values, in addition to acting as a barometer of precision, serve as a built-in mechanism for terminating the training process. Essentially, the algorithm's training continues until the validation loss function values exhibit no further significant changes. When the algorithm reaches a juncture where it can no longer reduce this loss function, the training process gracefully concludes.

The context of our research, the algorithm achieved a remarkable validation of the loss function after an exhaustive 3873 rounds of training, yielding a minimal loss value of 0.025. This feat underscores the algorithm's exceptional accuracy, which translates to an impressive 0.975.

For a visual representation of the algorithm's dynamic performance throughout each training round, please refer to Figures 6 and 7. These figures vividly illustrate the fluctuations in the loss function and the accuracy of the algorithm during its training iterations.

Notably, it's worth mentioning that the training process for this algorithm spanned a duration of 20 hours, 48 minutes, and 27 seconds using a core i9 12900E system of 32GB RAM. This timeframe holds significant merit, especially when considering the substantial volume of data involved. One contributing factor

to this efficiency is the utilization of the computer's graphics processing unit (GPU) for algorithmic computations, as opposed to relying solely on the central processing unit (CPU). Nevertheless, it's crucial to acknowledge that hardware specifications can exert a considerable influence on the duration of the training process. Additionally, the process of batching data, while necessary, introduces a delay as information is progressively transmitted to the algorithm's processing unit or kernel, which can affect overall processing time.

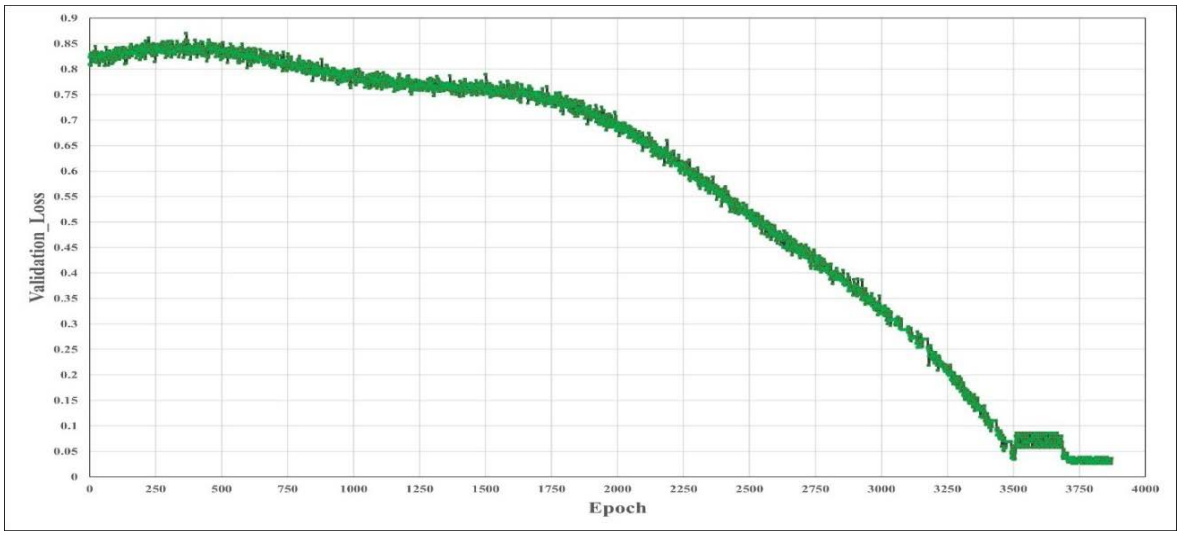

Figure 6—Validation loss per Epoch

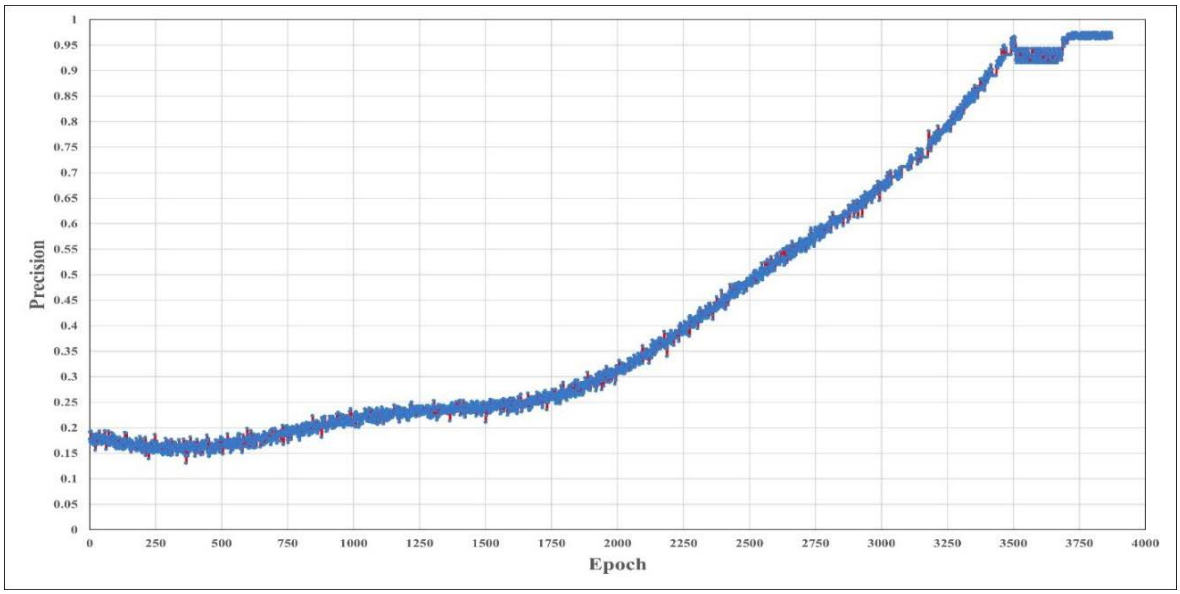

Figure 7—Precision per Epoch

One effective approach to gaining deeper insights into the algorithm's performance is through the examination and interpretation of its output graphs. The generative-adversarial algorithm stands as one of the most intricate and sophisticated entities in the realm of artificial intelligence. Consequently, deciphering the nuances presented in its output graphs serves as a crucial logbook, enabling us to develop a deeper understanding of its intricate subcomponents.

To facilitate this understanding, we turn our attention to the validation loss function, which serves as a powerful lens through which to scrutinize the algorithm's learning process. Figure 8, thoughtfully divided into three distinct sections based on the graph's slope, offers a comprehensive view of the algorithm's evolution.

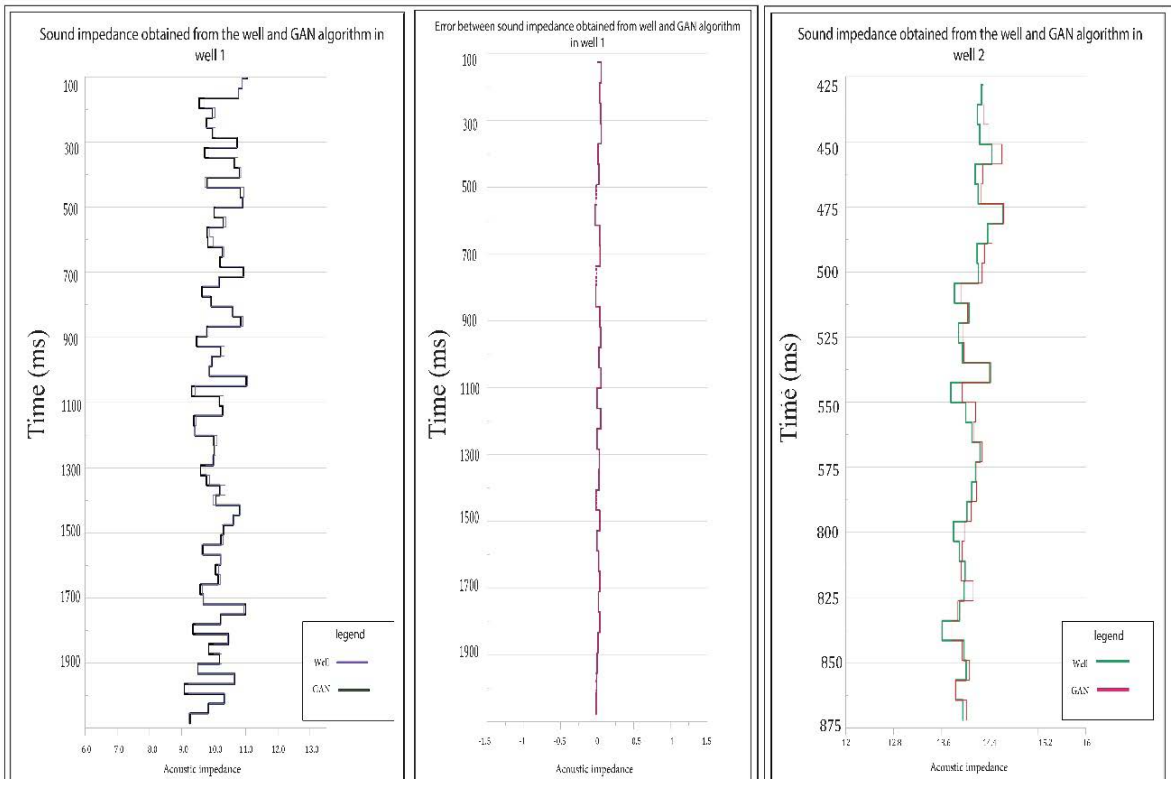

Figure 8—Segmented Validation loss chart

In the initial segment, the graph exhibits a subtle and gradual change in slope. Here, the generative algorithm is in the midst of its learning journey, skillfully crafting and generating sound resistance logs. Concurrently, the adversarial algorithm excels at distinguishing erroneous data from accurate ones with remarkable precision.

Transitioning into the second segment, we witness the generator algorithm's progression as it refines its log-generation capabilities. However, a noticeable interruption occurs at the juncture marking the transition from section 2 to section 3. This disruption is the result of the activation of a critical safeguard: the learning protection algorithm. This ingenious mechanism combats overfitting by intermittently deactivating specific neurons within the algorithm. This proactive approach prevents the algorithm from becoming overly specialized, ensuring its adaptability to diverse data patterns.

Finally, in the third segment, we observe a harmonious equilibrium between the adversarial and generating algorithms. This delicate balance reflects the algorithm's capacity to produce accurate, high-quality results while maintaining

data integrity. In essence, these visual insights into the algorithm's performance, as exemplified by Figure 8, provide an invaluable window into the inner workings of this complex AI system, shedding light on its multifaceted learning dynamics and fine-tuned self-regulation mechanisms.

As elucidated in preceding sections, our well dataset comprises a total of 15 wells, 10 of which played a pivotal role in the algorithm's training process, while the remaining 5 wells were meticulously reserved for algorithmic testing. It is of paramount importance to highlight that these 5 wells, along with their proximate seismic trace, remained unseen by the algorithm. In other words, the information pertaining to these specific wells and their associated seismic trace was intentionally excluded from the data collection process.

To ensure that the algorithm's results align seamlessly with the scale of the well data, a meticulous procedure was followed. Firstly, the acoustic impedance profiles within each well were diligently calculated. Subsequently, these results were skillfully transformed to match the seismic scale in close proximity to the well, utilizing a Backus averaging technique. Following this critical step, the aftershocks near each well were procured as requested data inputs for the data-adversarial algorithm. The algorithm then generated the inverse, namely the acoustic impedance, which was rigorously evaluated against the acoustic impedance derived directly from the well logging data. The outcomes of this rigorous evaluation have proven to be exceptionally satisfying, a fact that will become increasingly evident as we delve further into our findings.

A conscious effort was made to ensure that the selection of the utilized wells was not constrained to a single geographic region or a limited time range. This strategic decision was driven by the objective of attaining algorithmic results that encompass a broad spectrum, spanning both high and low values of acoustic impedance.

Figures 9 and 10 present visual representations of the acoustic impedance estimations juxtaposed with the sound resistance derived directly from well logging. Moreover, each estimation is accompanied by its respective error rate. The mean squared error (MSE) values reveal the accuracy of the algorithm's predictions. For instance, for well number one, the MSE equates to 0.10615 acoustic impedance units, while for well number two, it stands at 0.10819 acoustic impedance units. This pattern continues, with the MSE values for each well illustrating the algorithm's proficiency in estimating acoustic impedance across the dataset. Notably, for well number thirty-five, the MSE amounts to 0.10169 acoustic impedance units, for well number thirty-seven, it reaches 0.12529 acoustic impedance units, and lastly, for well number fifty, it registers at 0.11555 acoustic impedance units.

These results underscore the algorithm's remarkable capacity to approximate acoustic impedance values, demonstrating its robustness and reliability across a diverse array of well data scenarios.

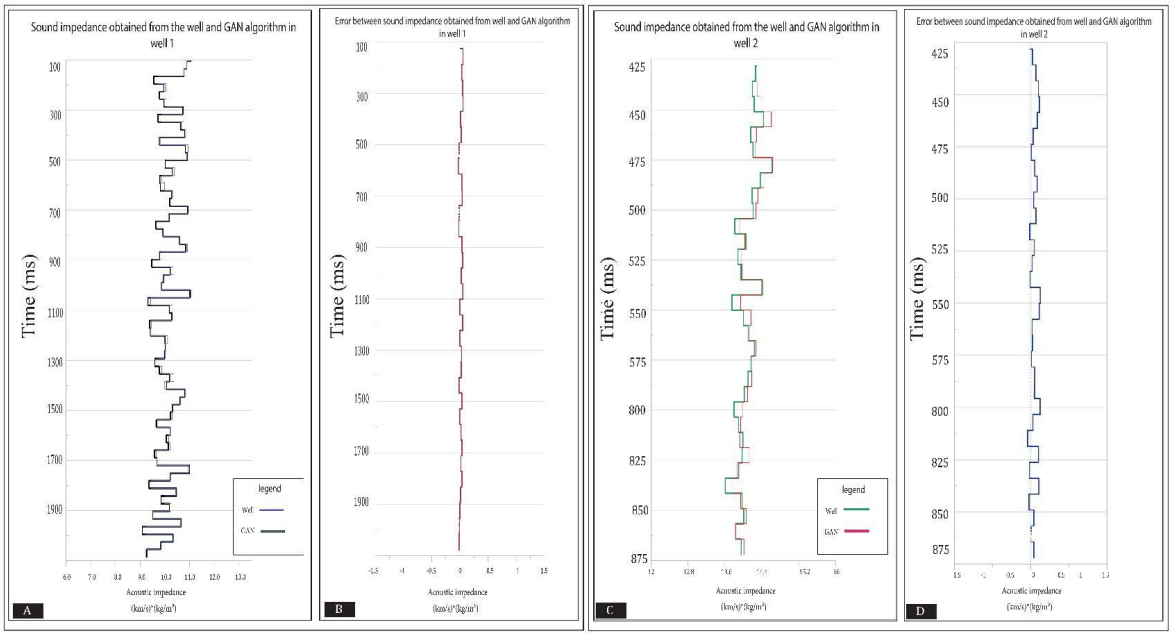

Figure 9— Comparing the impedance obtained from the well and the GAN algorithm along with its error. (A&B) Well No.1; (C&D) Well No.2

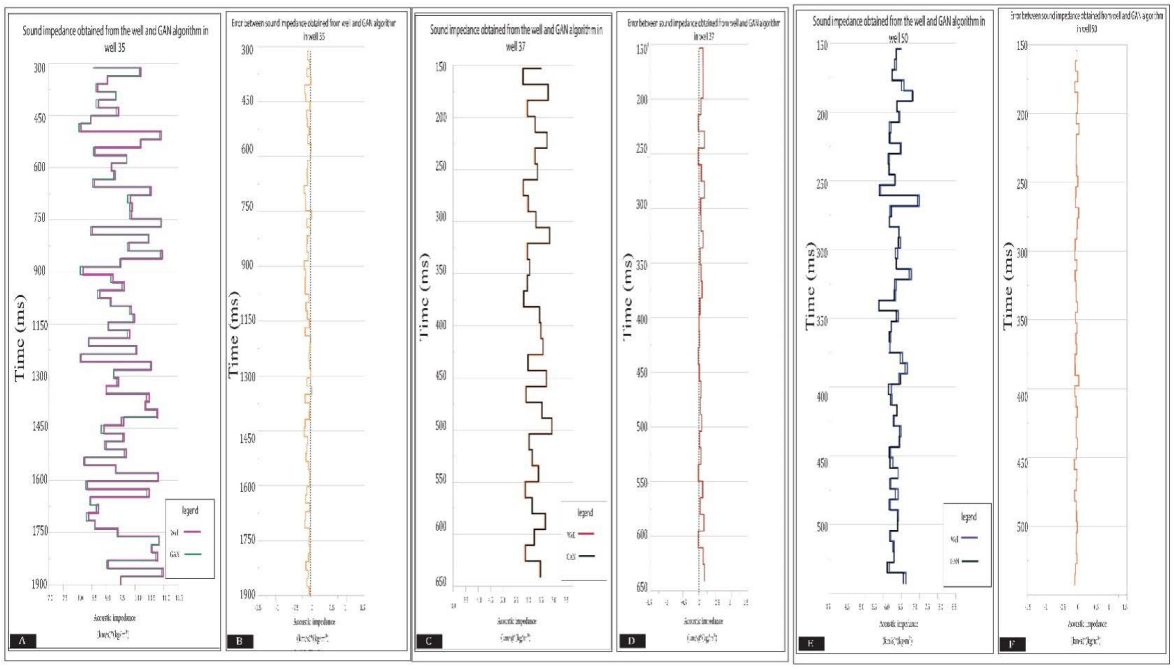

Figure 10— Comparing the impedance obtained from the well and the GAN algorithm along with its error. (A&B) Well No.35; (C&D) Well No.37; (E&F) Well No.50

Following the inversion of the seismic cube, we arrive at the ensuing results, which are meticulously detailed in Figures 11 and 12.

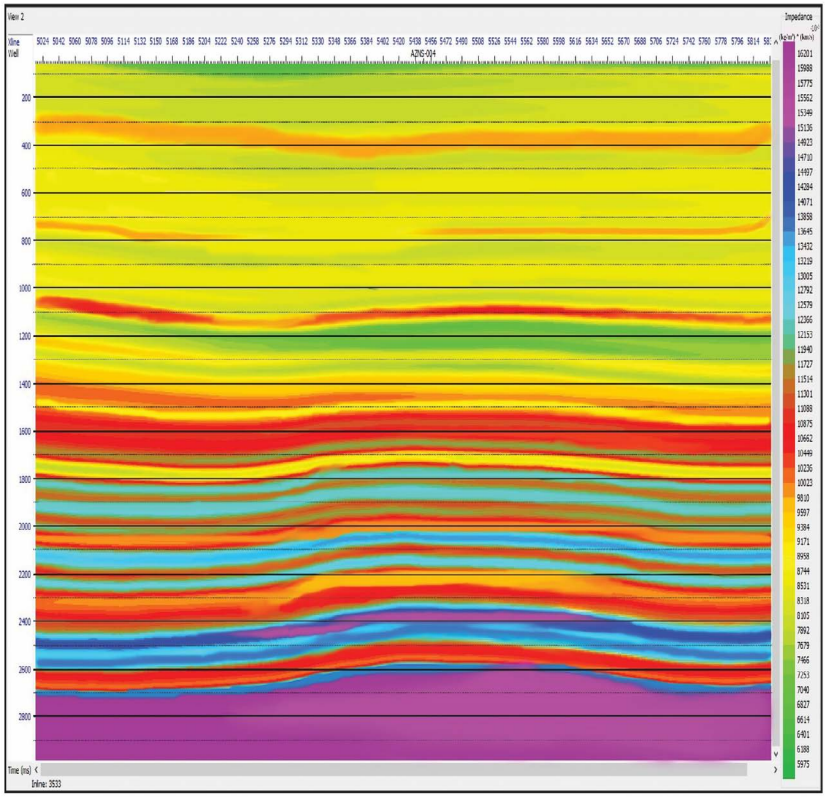

Figure 11—In-line number 3533-GAN Inversion results

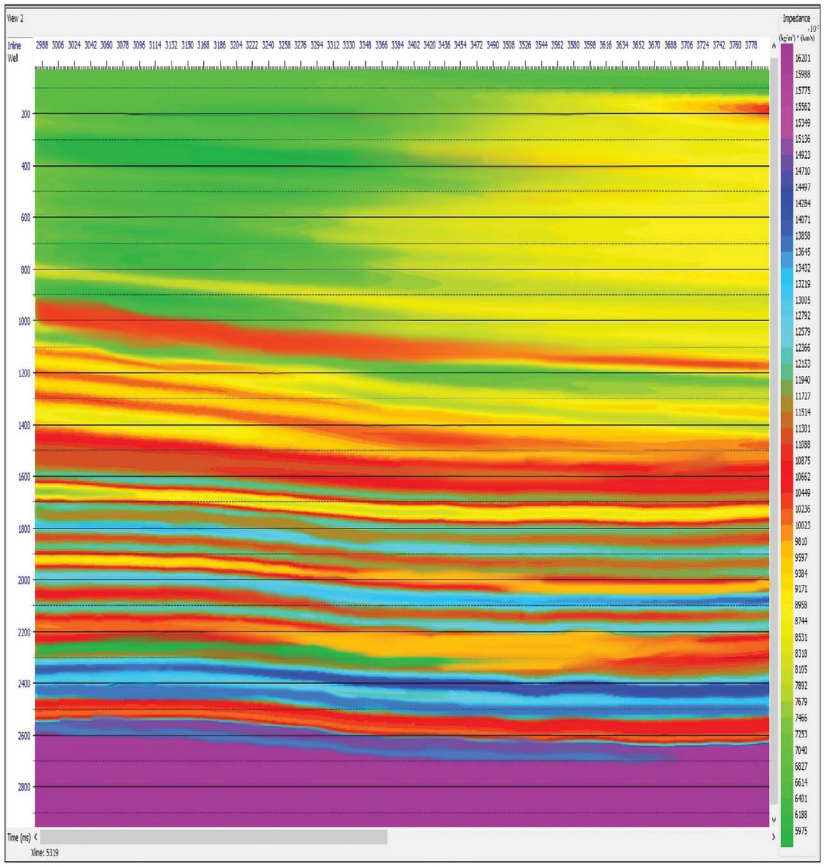

Figure 12—X-line number 5319 – GAN Inversion results

In seismic inversion, the generative-adversarial algorithm differs significantly from traditional methods in various aspects. One of the most notable distinctions is its liberation from the need for wavelet extraction, a key characteristic that sets it apart. Traditional approaches often involve wavelet extraction, which introduces a potential compromise in result accuracy. This is due to the manual intervention required during wavelet preparation, where human operators iterate to identify the most suitable wavelet. As a result, traditional seismic inversion outcomes bear the mark of human skill and precision.

Moreover, the noise in seismic and well-logging operations poses a persistent challenge. Many traditional methods are susceptible to noise interference, which can jeopardize result fidelity. Excessive noise levels can render the entire dataset untrustworthy, necessitating data acquisition repetition. In contrast, when using the generative-adversarial deep learning algorithm for inversion, the need for wavelet extraction is entirely eliminated. The inversion process is based on generating a log at the location of each trace, followed by computing the acoustic impedance log. As a result, there is no requirement for external wavelet extraction, as the generative-adversarial algorithm inherently possesses the ability to learn. Post-training, it can effectively distinguish between noise and the original data, significantly mitigating the impact of noise. During the training phase, the algorithm acquires the capability to discern the interplay between different data components and, thanks to its memory, diminishes noise interference during the production phase. Notably, the inversion method using the generative-adversarial algorithm differs from the color inversion method as it eliminates the need for secondary operator calculations, offering a more streamlined and accessible workflow. In the subsequent sections, we will delve into the outcomes of inversion achieved through the generative-adversarial algorithm, comparing them with band-limited methods and model-based inversion to further highlight the distinctive capabilities of this algorithm (Figure 13 and 14).

In stark contrast to the outcomes produced by the band-limited methods and model-based inversion, the results generated by the generative-adversarial algorithm exhibit an exceptional level of coherence. This heightened coherence signifies that the inversion results are characterized by a remarkable absence of discontinuities and non-uniformities. The underlying rationale for this remarkable consistency lies in the intrinsic memory of the generative algorithm.

The generative algorithm embarks on the construction of new structures by diligently referencing the precedents it has encountered. This memory-driven approach imparts a unique advantage, ensuring that the results remain harmonious and steadfastly coherent. The visual representation in Figure 13 distinctly underscores the divergent nature of the inversion outcomes across these three approaches. This marked difference in the outcomes can be predominantly attributed to the generative-adversarial algorithm's innate capacity for learning and adaptability. As the algorithm proceeds through its

iterations, it progressively hones its ability to discern and replicate structural patterns, thus underpinning the consistent and coherent nature of its inversion results.

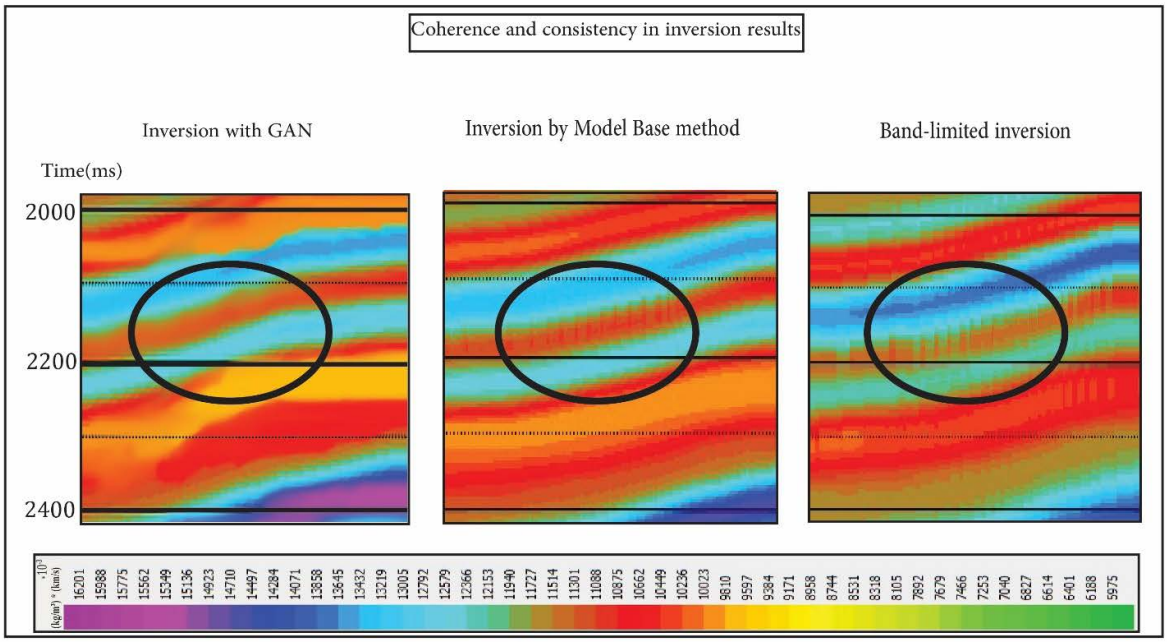

Figure 13—Comparing the consistency of seismic inversion results using three GAN algorithms, band limited and model base methods.

The generative-adversarial algorithm stands out as a powerful tool, and its effectiveness is enhanced through training with well survey data. What further distinguishes it and significantly elevates its appeal is its superior resolution when compared to conventional methods. It's crucial to emphasize that while the resolution of the generative-adversarial algorithm's results may align with the seismic wavelength, it is precisely this alignment that results in a substantial distinction in outcomes. The core of this algorithm's effectiveness lies in the nuanced functioning of its adversarial unit, known as the discriminator. In its dynamic interaction with the generator network, the discriminator plays a pivotal role in augmenting and optimizing the fidelity of the data it processes. The result of this synergy is a marked improvement in the correlation between the algorithm's results and real-world data, effectively enhancing both vertical and lateral resolution. As elegantly illustrated in Figure 14, the generative-adversarial algorithm excels in delivering vertical resolution and clearly showcases its prowess in lateral resolution. This profound enhancement in resolution capabilities signifies a significant leap forward compared to conventional inversion methods.

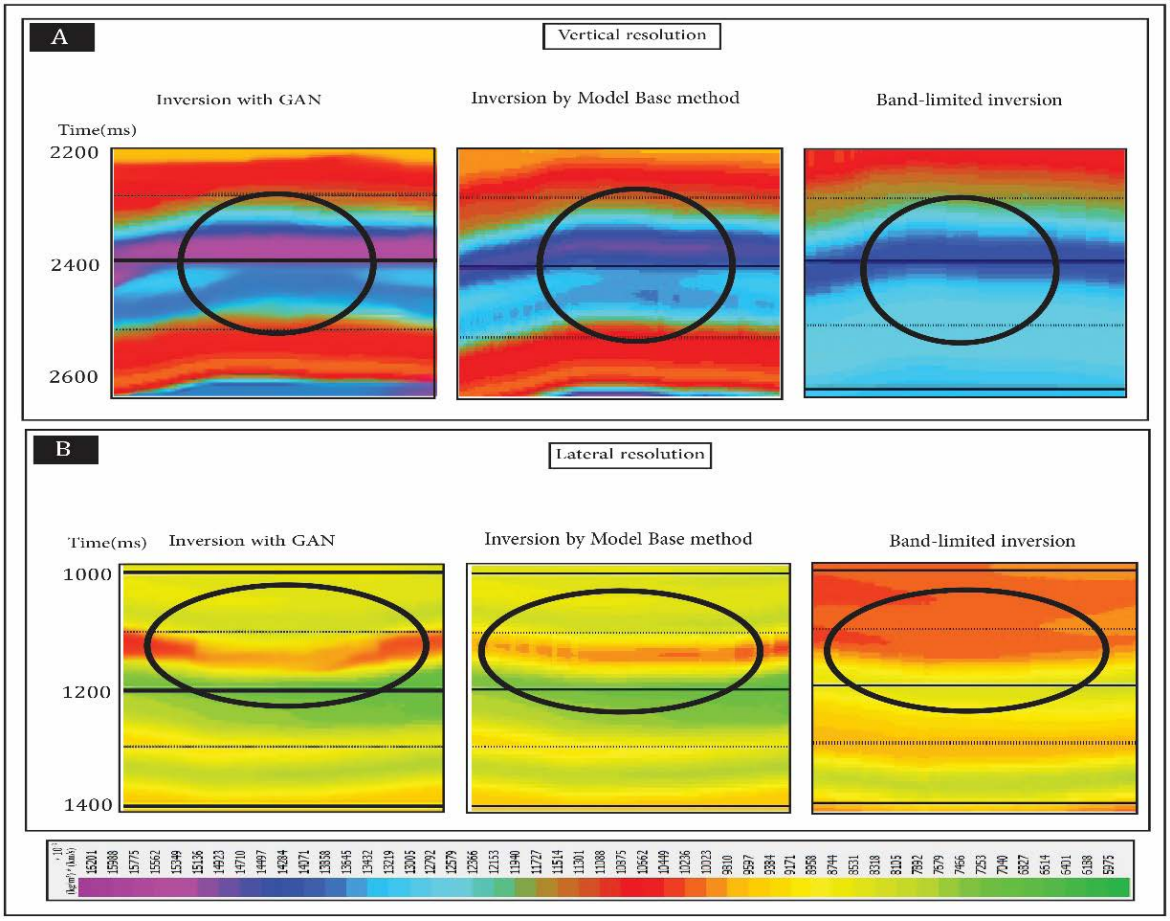

Figure 14—Compare resolution of seismic inversion results using three GAN algorithms methods, band limited method and model base method. (A) Vertical resolution; (B) lateral resolution.

In the forthcoming analysis, we investigate the correlation coefficients, which serve as a pivotal measure of alignment, between the datasets generated by the generative-adversarial algorithm and the acoustic impedance data extracted from within the well. In addition to this, we conduct an in-depth examination of the results obtained through the band-limited and model-base methods (Table4). This comprehensive evaluation is presented visually in Figures 15 to 19. It's noteworthy to emphasize that the five wells under study form a crucial component of test dataset. Significantly, the generative-adversarial algorithm was not previously exposed to this subset of data during its training. This crucial distinction underscores the algorithm's ability to generalize its learning to unseen data.

The correlation coefficients are as follows:

1. For well number 1, the correlation coefficient stands at 0.98918, suggesting a strong alignment between the algorithm's outputs and the well data.

2. For well number 2, the correlation coefficient is an impressive 0.96143, indicating a highly congruent match between the algorithmically generated data and the actual well measurements.

3. In the case of well number 35, a remarkable correlation coefficient of 0.98994 is achieved, underlining the robustness of the algorithm's predictions.

4. For well number 37, the correlation coefficient stands at 0.96657, suggesting a strong alignment between the algorithm's outputs and the well data.

5. Lastly, for well number 50, the correlation coefficient reaches a commendable 0.98174, reaffirming the algorithm's accuracy in replicating acoustic resistance values.

These results collectively emphasize the generative-adversarial algorithm's consistent ability to produce data that closely mirrors real-world acoustic impedance measurements, even when applied to unseen well data. This capability underscores the precision and reliability of the algorithm in various data contexts.

Table 4— correlation coefficient between the results of three methods of inversion with well data.

Methods of inversion	GAN	Model-base	Band -limited
Well No.1	**0.98918**	**0.65703**	**0.64175**
Well No.2	**0.96143**	**0.78652**	**0.66614**
Well No.35	**0.98994**	**0.83537**	**0.71285**
Well No.37	**0.96657**	**0.51795**	**0.46533**
Well No.50	**0.98174**	**0.65063**	**0.3534**

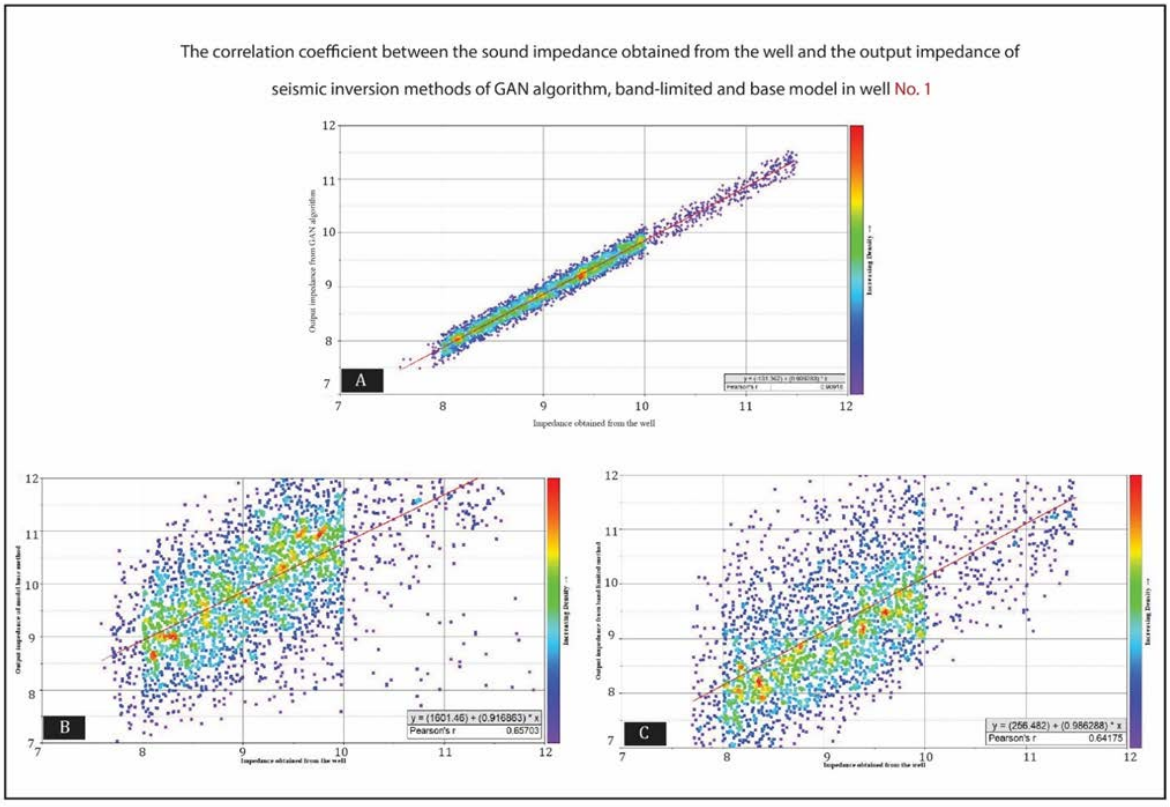

Figure 15—Correlation coefficient between the acoustic impedance obtained from well number 1 and the output impedance of seismic inversion methods of generator-adversarial algorithm, band limited and model-based. (A) GAN(B) Model-based method; (C) Band-Limited Method.

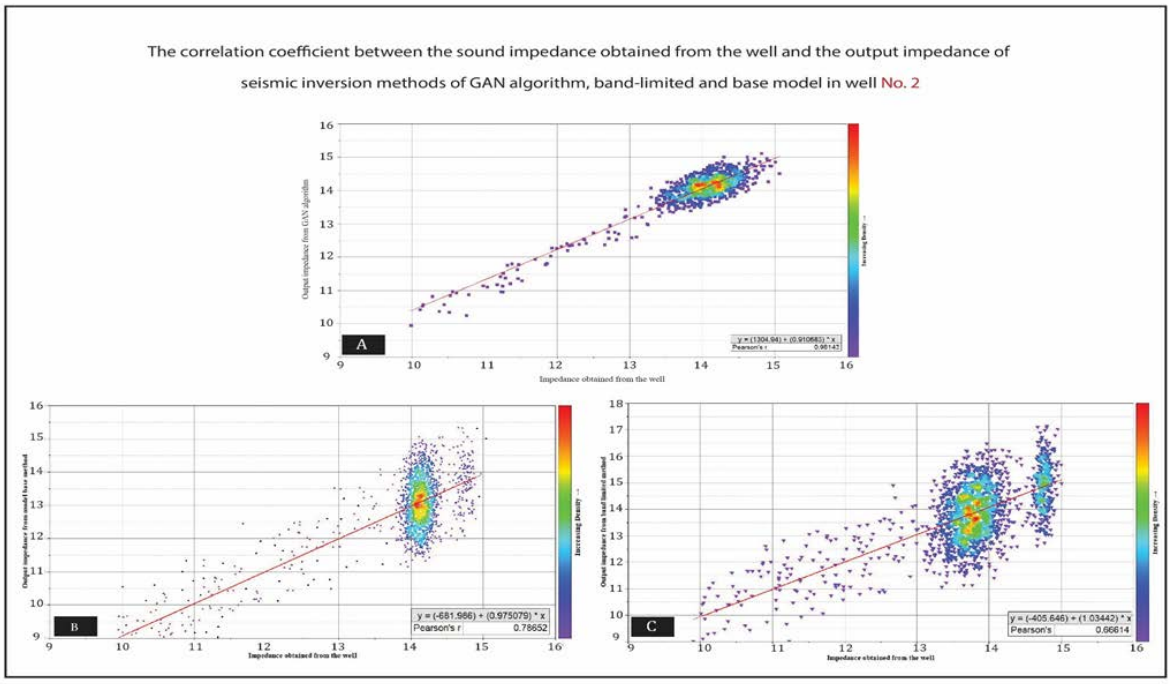

Figure 16— Correlation coefficient between the acoustic impedance obtained from well number 2 and the output impedance of seismic inversion methods of generator-adversarial algorithm, band limited and model-based. (A) GAN(B) Model-based method; (C) Band-Limited Method.

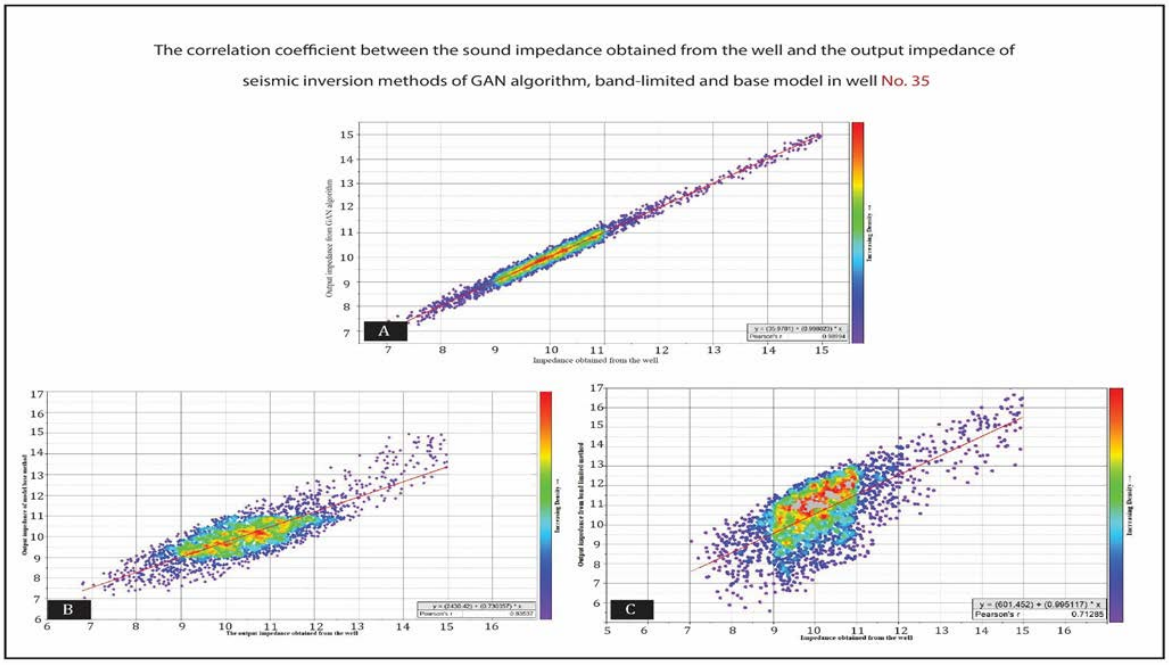

Figure 17— Correlation coefficient between the acoustic impedance obtained from well number 35 and the output impedance of seismic inversion methods of generator-adversarial algorithm, band limited and model-based. (A) GAN(B) Model-based method; (C) Band-Limited Method.

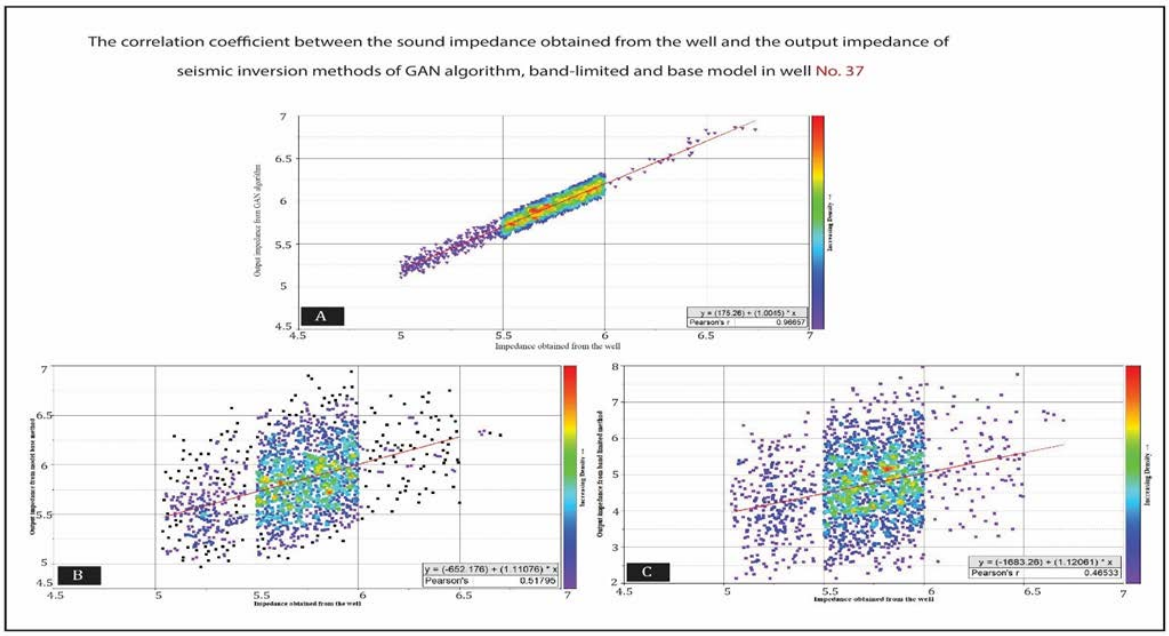

Figure 18— Correlation coefficient between the acoustic impedance obtained from well number 37 and the output impedance of seismic inversion methods of generator-adversarial algorithm, band limited and model-based. (A) GAN(B) Model-based method; (C) Band-Limited Method.

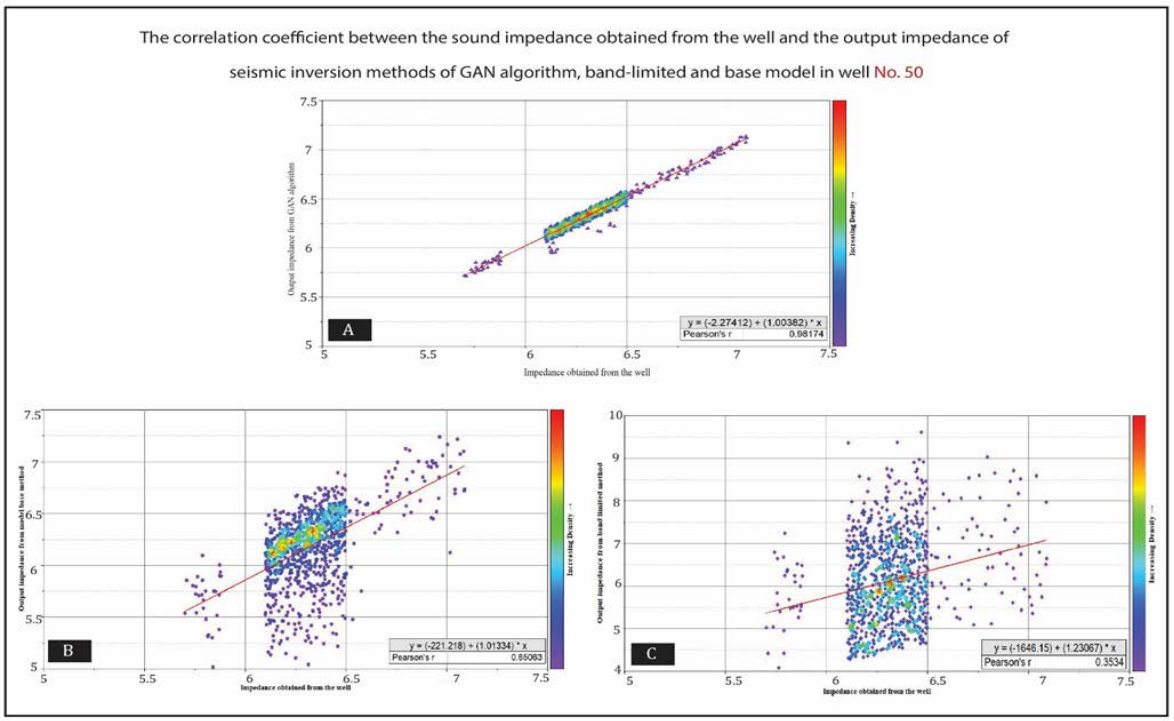

Figure 19— Correlation coefficient between the acoustic impedance obtained from well number 50 and the output impedance of seismic inversion methods of generator-adversarial algorithm, band limited and model-based. (A) GAN(B) Model-based method; (C) Band-Limited Method.

The table presented below (Table5) provides a comprehensive overview of MSE values, highlighting the performance of the GAN algorithm in the context of seismic inversion accuracy.

Table 5—MSE Values in Test Wells

Methods of inversion	Well 1	Well 2	Well35	Well 35	Well 50
GAN	**0.10615**	**0.10819**	**0.10169**	**0.12529**	**0.11555**
Model-base	**2.1501**	**2.1686**	**1.4504**	**3.8829**	**3.459**
Band -limited	**3.8641**	**2.8358**	**2.0356**	**4.8028**	**5.6773**

As evident from the above table, the GAN algorithm stands out by demonstrating significantly improved accuracy in seismic inversion when compared to both the model-base and the band limited algorithms across various test wells. Notably, the MSE values for the GAN algorithm are notably lower than those of the alternative models. This data underscores the potential of the GAN algorithm as a valuable tool in enhancing the precision of seismic inversion processes, suggesting its efficacy in real-world applications and its potential to contribute to advancements in the field. Further analysis and exploration of this algorithm's capabilities could yield valuable insights and benefits in geophysical exploration and related domains.

CONCLUSION

Seismic inversion is a highly effective technique for exploring hydrocarbon reserves, and continuous optimization and the development of new methodologies are essential for increasing productivity and mitigating risks in exploratory operations. In this landscape of progress, the Generative Adversarial Deep Learning algorithm has emerged as a cutting-edge and remarkably efficient tool for creating highly realistic models. When applied to seismic data inversion, this algorithm not only enhances precision but also streamlines computational efficiency. Moreover, its development within the Python programming ecosystem ensures accessibility to experts worldwide, fostering an open-source culture for further refinement and evolution. Despite its complex architecture, the Generative Adversarial algorithm is user-friendly, with the training and implementation phases compartmentalized, making seismic cube inversions as straightforward as a few simple clicks.

The Generative Adversarial Deep Learning algorithm is a powerful instrument for generating highly realistic models and significantly reducing errors in acoustic impedance measurements compared to conventional methods such as Band-limited and Model-based inversion, aligning closely with impedance values acquired from well data. It boasts exceptionally high vertical and lateral resolution capabilities in estimating acoustic impedances, enabling the discernment of subsurface layers based on impedance distinctions. Additionally, its structural robustness makes it resistant to noise, preventing error propagation caused by noise in the results. The GAN algorithm also exhibits a strong correlation between its output impedance and reality, with a maximum

Mean Squared Error (MSE) of 0.12529 acoustic impedance units compared to 5.6773 in other inversion methods, achieving an accuracy of 97.5%.

For future research, optimizing temporary memory management is essential to prevent bottlenecks and enhance algorithm training efficiency. Exploring more efficient alternatives to the Backus algorithm can reduce code complexity and improve accuracy. Comparative analyses with other deep learning and machine learning methods can refine the algorithm and highlight its strengths. Investigating new sub-network architectures beyond fully connected networks shows promise, potentially revealing novel insights and improving performance.

In conclusion, the Generative Adversarial Deep Learning algorithm represents a promising frontier in seismic inversion and subsurface exploration. Its potential for refinement and development, coupled with its robustness and efficiency, makes it a valuable tool for both current and future experts in the field. Further research and innovation in this domain hold the key to unlocking even greater insights and capabilities in hydrocarbon reserve exploration.

REFERENCES

Habibullah, M., Mohebian, M., Soolanayakanahally, R., Wahid, K., & Dinh, A. (2020). A Cost-Effective and Portable Optical Sensor System to Estimate Leaf Nitrogen and Water Contents in Crops. *Sensor, 20*(5). doi:https://doi.org/10.3390/s20051449

Helgesen, J., Magnus, I., Prosser, S., Saigal, G., Aamodt, G., & Dolberg, D. (2000). Comparison of constrained sparse spike and stochastic inversion for porosity prediction at Kristin Field. *The Leading Edge, 19*(4), 400-407. doi:https://doi.org/10.1190/1.1438620

Ji, Y., Yuan, S., & Wang, S. (2019). Multi-trace stochastic sparse-spike inversion for reflectivity. *Journal of Applied Geophysics, 161*, 84-91. doi:https://doi.org/10.1016/j.jappgeo.2018.12.006

Lin, Y., Theiler, J., & Wohlberg, B. (2023). Physics-Guided Data-Driven Seismic Inversion: Recent progress and future opportunities in full-waveform inversion. *IEEE Signal Processing Magazine, 40*(1), 115-133. doi:https://doi.org/10.1109/MSP.2022.3217658

Mallick, S. (1995). Model-based inversion of amplitude-variations-with-offset data using a genetic algorithm. *GEOPHYSICS, 60*(4), 939-954. doi:https://doi.org/10.1190/1.1443860

Zhu, Z., Chen, X., Ren, H., Tao, L., Jiang , J., Wang, T., . . . Du, R. (2022). Seismic Facies Analysis Using the Multiattribute SOM-K-Means Clustering. *Computational intelligence and neuroscience*. doi:https://doi.org/10.1155/2022/1688233

Aggarwal, A., Mittal, M., & Battineni , G. (2021). Generative adversarial network: An overview of theory and applications. *International Journal of Information Management Data Insights, 1*(1). doi:https://doi.org/10.1016/j.jjimei.2020.100004

Azizzadeh Mehmandost Olya, B., & Mohebian, R. (2023a). Hydrocarbon reservoir potential mapping through Permeability estimation by a CUDNNLSTM Deep Learning Algorithm. *International Journal of Mining and Geo-Engineering*. doi:10.22059/IJMGE.2023.356428.595045

Azizzadeh Mehmandost Olya, B., & Mohebian, R. (2023b). Q-FACTOR ESTIMATION FROM VERTICAL SEISMIC PROFILING (VSP) WITH DEEP LEARNING ALGORITHM, CUDNNLSTM. *JOURNAL OF SEISMIC EXPLORATION, 32*, 89-104.

Azizzadeh Mehmandost Olya, B., Mohebian, R., & Moradzadeh, A. (2024a). Seismic inversion using the Generative-Adversarial algorithm for hydrocarbon exploration. *The 9th International Conference Chemical, Petroleum and Environmental* (p. https://civilica.com/doc/1949772/). Tehran: civilica.

Azizzadeh Mehmandost Olya, B., Mohebian, R., Bagheri, H., Mahdavi, A., & Khan Mohammadi, A. (2024b). Toward Real-time Fracture Detection on Image Logs Using Deep Convolutional Neural Networks, YoloV5. *Interpretation, 12*(2), SB9-SB18. doi:https://doi.org/10.1190/INT-2022-0104.1

Backus, G. (1962). Long-wave elastic anisotropy produced by horizontal layering. *Journal of Geophysical Research, 67*(11), 4427-4440.

Bagheri, H., Mohebian, R., Moradzadeh, A., & Azizzadeh Mehmandost Olya, B. (2024). Pore size classification and prediction based on distribution of reservoir fluid volumes utilizing well logs and deep learning algorithm in a complex lithology. *Artificial Intelligence in Geosciences, 5*, 100094. doi:https://doi.org/10.1016/j.aiig.2024.100094

Bahramali Asadi Kelishami , S., & Mohebian, R. (2021). Petrophysical rock typing (PRT) and evaluation of Cenomanian–Santonian lithostratigraphic units in southwest of Iran. *Carbonates and Evaporites, 36*. doi:https://doi.org/10.1007/s13146-020-00669-3

Chopra, S., & Marfurt, K. J. (2005). Seismic attributes — A historical perspective. *Geophysics, 70*(5), 1SO-Z82. doi:https://doi.org/10.1190/1.2098670

Creswell, A., White, T., Dumoulin, V., Arulkumaran, K., Sengupta, B., & Bharath, A. (2018). Generative adversarial networks: An overview. *IEEE signal processing magazine, 35*(1), 53-65. doi:https://doi.org/10.1109/MSP.2017.2765202

Ferguson, R., & Margrave, G. (1996). A simple algorithm for band-limited impedance inversion. *CREWES Research Report, 8*(21), 1-10.

Frank, J., Eisenhofer, T., Schönherr, L., Fischer, A., Kolossa, D., & Holz, T. (2020). Leveraging frequency analysis for deep fake image recognition. *International conference on machine learning* (pp. 3247-3258). PMLR.

Geng, Z., & Wang, Y. (2020). Automated design of a convolutional neural network with multi-scale filters for cost-efficient seismic data classification. *Nature communications, 11*(1). doi:https://doi.org/10.1038/s41467-020-17123-6

Gogoi, T., & Chatterjee, R. (2019). Estimation of petrophysical parameters

using seismic inversion and neural network modeling in Upper Assam basin, India. *Geoscience Frontiers, 10*(3), 1113-1124. doi:https://doi.org/10.1016/j.gsf.2018.07.002

Goodfellow, I., Pouget-Abadie, J., Mirza, M., Xu, B., Warde-Farley, D., Ozair, S., . . . Bengio, Y. (2014). Generative adversarial nets. *Advances in neural information processing systems, 27*.

Gui, J., Sun, Z., Wen, Y., Tao, D., & Ye, J. (2021). A Review on Generative Adversarial Networks: Algorithms, Theory, and Applications. *IEEE Transactions on Knowledge and Data Engineering, 35*(4). doi:https://doi.org/10.1109/TKDE.2021.3130191

Karras, T., Aittala, M., Hellsten, J., Laine, S., Lehtinen, J., & Aila, T. (2020). Training generative adversarial networks with limited data. *Advances in neural information processing systems, 33*, 12104-12114.

King, R. (1992). High-resolution shallow seismology: history, principles and problems. *Quarterly Journal of Engineering Geology and Hydrogeology, 25*(3), 177-182. doi:https://doi.org/10.1144/GSL.QJEG.1992.025.03.01

Kushwaha, P., Maurya, S., & Singh, N. (2020). Use of maximum likelihood sparse spike inversion and probabilistic neural network for reservoir characterization: a study from F-3 block, the Netherlands. *Journal of Petroleum Exploration and Production Technology, 10*, 829-845. doi:https://doi.org/10.1007/s13202-019-00805-3

Lin, Y., Theiler, J., & Wohlberg, B. (2023). Physics-Guided Data-Driven Seismic Inversion: Recent progress and future opportunities in full-waveform inversion. *IEEE Signal Processing Magazine, 40*, 115-133. doi:10.1109/MSP.2022.3217658.

Liu, H.-B., & Lee, I. (2020). MPL-GAN: Toward realistic meteorological predictive learning using conditional GAN. *IEEE Access 8, 8*, 93179-93186. doi:https://doi.org/10.1109/ACCESS.2020.2995187

Maurya, S., & Singh, K. (2017). Band limited impedance inversion of Blackfoot field, Alberta, Canada. *Geophysics, 38*(1), 57-61.

Mintrop, L. (1949). On the stratification of the Earth's crust according to seismic studies of a large explosion and of earthquakes. *Geophysicists, 14*(3), 321-336. doi:https://doi.org/10.1190/1.1437540

Mohebian, R., Bagheri, H., Kheirollahi, M., & Bahrami, H. (2021). Permeability Estimation Using an Integration of Multi-Resolution Graph-based Clustering and Rock Typing Methods in an Iranian Carbonate Reservoir. *Journal of Petroleum Science and Technology, 11*(3), 49-58. doi:10.22078/jpst.2022.4737.1785

Moradi Chaleshtori, Y., Yarmohammadi, S., Mohebian, R., & Azizzadeh Mehmandost Olya, B. (2024). Maximizing of the coverage and quality in micro resistivity image log by applying minimum weighted norm interpolation and anisotropic diffusion filter. *International Journal of Mining and Geo-Engineering*, 221-227.

Rajabi, A., Mahmoodi, P., Rastad, E., Niromand, S., Peernajmodin, P., Akbari, Z., . . . Haghi, A. (2019). A review of fluid inclusion investigations on

Cretaceous sediment-hosted Zn-Pb (±Ba±Fe±Ag±Cu) deposits in the Malayer-Esfahan metallogenic belt (MEMB). *Third Biennial Iranian National Fluid Inclusion conference*.

Russell, B. (1988). *Introduction to seismic inversion.* SEG Books. Sheriff, R., & Gedart, L. (1995). *Exploration seismology.* Cambridge university press.

Virieux , J., & Operto, S. (2009). An overview of full-waveform inversion in exploration geophysics. *GEOPHYSICS, 74*(6), 1ND-Z107. doi:https://doi.org/10.1190/1.3238367

Wang, Y.-Q., Wang, Q., Kai Lu, W., Ge, Q., & Yan , X.-F. (2022). Seismic impedance inversion based on cycle-consistent generative adversarial network. *Petroleum Science, 19*(1), 147-161. doi:https://doi.org/10.1016/j.petsci.2021.09.038

Xu, L., Skoularidou, M., Cuesta-Infante, A., & Veeramachaneni, K. (2019). Modeling tabular data using conditional gan. *Advances in neural information processing systems,, 32*.

Xu, S., Wang, D., Chen, F., Zhang, Y., & Lambare, G. (2012). Full Waveform Inversion for Reflected Seismic Data. *74th EAGE Conference and Exhibition incorporating EUROPEC 2012.* European Association of Geoscientists & Engineers. doi:https://doi.org/10.3997/2214-4609.20148725

Yilmaz, O. (2001). *Seismic data analysis: Processing, inversion, and interpretation of seismic data.* Society of exploration geophysicists.

Zhang, Y., Zhu, X., & Gao, J. (2023). Seismic Inversion Based on Acoustic Wave Equations Using Physics-Informed Neural Network. *IEEE Transactions on Geoscience and Remote Sensing, 61*, 1-11. doi:https://doi.org/10.1109/TGRS.2023.3236973